Boron–Diindomethene (BDI) Dyes and Their Tetrahydrobicyclo Precursors—en Route to a New Class of Highly Emissive Fluorophores for the Red Spectral Range

Zhen Shen,[a, d] Holger Röhr,[b, e] Knut Rurack,*[b] Hidemitsu Uno,[c] Monika Spieles,[b] Burkhard Schulz,[b] Günter Reck,[b] and Noboru Ono*[a]

Abstract: The X-ray crystallographic, optical spectroscopic, and electrochemical properties of a newly synthesized class of boron–diindomethene (BDI) dyes and their tetrahydrobicyclo precursors (bc-BDP) are presented. The BDI chromophore was designed to show intensive absorption and strong fluorescence in an applicationary advantageous spectral range. Its modular architecture permits fusion of a second subunit, for example, a receptor moiety to the dye's core to yield directly linked yet perpendicularly prearranged composite systems. The synthesis was developed to allow facile tuning of the chromophore platform and to thus adjust its redox properties. X-ray analysis revealed a pronounced planarity of the chromophore in the case of the BDIs, which led to a remarkable close packing in the crystal of the simplest derivative. On the other hand, deviation from planarity was found for the diester-substituted bc-BDP benzocrown that exhibits a "butterfly"-like conformation in the crystal. Both families of dyes show charge- or electron-transfer-type fluorescence-quenching characteristics in polar solvents when equipped with a strong donor in the *meso*-position of the core. These processes can be utilized for signaling purposes if an appropriate receptor is introduced. Further modification of the chromophore can invoke such a guest-responsive intramolecular quenching process, also for receptor groups of low electron density, for example, benzocrowns. In addition to the design of various prototype molecules, a promising fluoroionophore for Na^+ was obtained that absorbs and emits in the 650 nm region and shows a strong fluorescence enhancement upon analyte binding. Furthermore, investigation of the remarkable solvatokinetic fluorescence properties of the "butterfly"-like bc-BDP derivatives suggested that a second intrinsic nonradiative deactivation channel can play a role in the photophysics of boron–dipyrromethene dyes.

Keywords: charge transfer · dyes/pigments · electron transfer · fluorescence

Introduction

The search for new fluorophores that absorb and emit in the red visible and/or near infrared (NIR) region of the spectrum is of continuing interest in many different fields of chemistry, ranging from optical spectroscopy-based sensing[1] through imaging applications[2] to materials chemistry related issues,[3] such as molecular switches and devices,[4] lasing media,[5] or electrooptical applications.[6] In addition to the wavelength range of operation, the key requirements for fluorescent dyes to be suitably employable in such fields are efficiency, in terms of a high extinction coefficient, a high rate of conversion of absorbed photons into emitted photons, and versatility with respect to the dye's synthesis as well as to its functionalization. A promising starting point for the construction of dyes showing intense and well-defined absorption bands in the red and/or NIR spectral range is the cyanine chromophore (Cy; Scheme 1).[7] In these dyes, according to the triad principle of colored organic compounds[8] and the concept of the (ideal) polymethine state,[9] the position of the absorption band depends on and can

[a] Dr. Z. Shen, Prof. N. Ono
Department of Chemistry, Faculty of Science
Ehime University, Matsuyama 790—8577 (Japan)
Fax: (+81) 899279590
E-mail: ononbr@dpc.ehime-u.ac.jp

[b] Dipl.-Phys. H. Röhr, Dr. K. Rurack, M. Spieles, B. Schulz, Dr. G. Reck
Div. I.3 Bundesanstalt für Materialforschung und -prüfung (BAM)
Richard-Willstätter-Strasse 11, 12489 Berlin (Germany)
Fax: (+49) 308-104-5005
E-mail: knut.rurack@bam.de

[c] Prof. H. Uno
Integrated Center for Science, Faculty of Science
Ehime University, Matsuyama 790—8577 (Japan)

[d] Dr. Z. Shen
Present address:
State Key Laboratory of Coordination Chemistry
Nanjing University, Nanjing 210093 (China)

[e] Dipl.-Phys. H. Röhr
Associated with: Fachbereich Biologie, Chemie, Pharmazie
Freie Universität Berlin, Takustrasse 3, 14195 Berlin (Germany)

Supporting information for this article is available on the WWW under http://www.chemeurj.org/ or from the author.

 DOI: 10.1002/chem.200400173

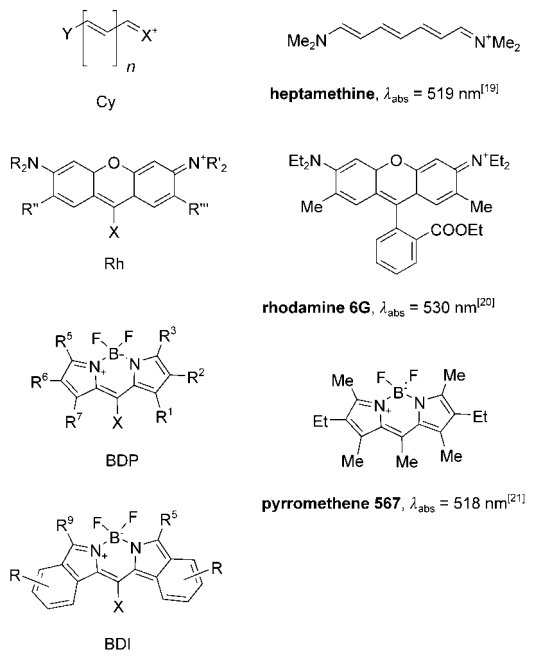

Scheme 1. General structure of the cyanine (Cy), rhodamine (Rh), boron–dipyrromethene (BDP; with the zwitterionic character indicated), and boron–diindomethene (BDI) chromophores. In the majority of actual examples, X and Y are heterocyclic or aromatic substitutents. For Rh, R to R‴ are mostly short alkyl substituents or hydrogens. For BDP and BDI, the substituents R^n can vary from H to alkyl and other small functional groups, or to larger aryl moieties. Three representative examples are included on the right.

thus be tuned by the number of vinylene groups *n* in the chain ("vinylene shift").[10] However, whereas a vast number of cyanine dyes have been synthesized so far and absorption maxima up to 1500 nm have been realized,[11] the fluorescence quantum yield of cyanines does not generally exceed 0.50 (for certain di- or trimethines) and drops rapidly with a further decrease towards monomethines or with an increase in the chain length.[12] This effect can be caused by various factors that are predominantly connected to the (multiple) flexible bonds of the molecules. For instance, twisting of single and/or double bonds can readily dissipate the excitation energy.[13] Other researchers identified the many vibrational degrees of freedom as a major nonradiative pathway for flexible and semiflexible cyanines.[14] Even for largely rigid or bridged cyanines, the remaining flexible bonds can still be an effective funnel for nonemissive deactivation.[15] In analogy to rhodamine (Rh) chemistry (for the chemical structure, see Scheme 1),[16] only the complete fixation of the chromophoric system seems to guarantee an intrinsically high conversion of the absorbed light into fluorescence emission.[17] However, the disadvantages here are the time-consuming and often complex synthesis of fully rigid cyanines and, in the case of the rhodamines, that the remaining positions for functionalization at the chromophoric core are limited. Moreover, as positively charged ions, the solubility of rhodamines is generally restricted to highly polar solvents and, for any application, the presence of the dye's counterion has to be taken into account.[18]

As an alternative, the internally zwitterionic boron–dipyrromethene (BDP) chromophore (Scheme 1) has gained considerable attention during the last three decades.[22] BDPs are rigid cyanine-type dyes with a fixed planarity of the chromophoric π-electron system. They combine the favorable properties of cyanines, such as their typical spectral shapes in absorption and emission, high molar extinction coefficients (usually $\varepsilon > 80{,}000\,\mathrm{M^{-1}\,cm^{-1}}$), and high fluorescence quantum yields (commonly $\Phi_f > 0.70$), while absorbing and emitting in the range of the simple heptamethine and rhodamine dyes (Scheme 1), or fluorescein dyes.[23] Additionally, the BDP core has a relatively moderate redox potential, which is a prerequisite when aiming at the construction of fluorescent switches based on electron- (ET) or charge-transfer (CT) processes.[22d,24] Owing to their specific chemical nature, BDPs are generally well soluble in a large variety of common solvents of different polarity. Despite these advantageous features, the spectral properties of the classical BDP chromophore are limited to the wavelength range between 470 and 530 nm. However, with regard to various applications it would be very interesting to have BDP dyes available that absorb and emit at longer wavelengths. For instance, in chemical sensing and imaging or for optical switches, the matrix can spectroscopically interfere at wavelengths ≤ 600 nm.[1e] Thus, other groups[25,26] and our group[27] have recently shifted the absorption and fluorescence maxima to longer wavelengths by chemical modification of the BDP core with aryl or styryl substituents, or have restricted bond rotation in rigid ring-fused systems. Here, the constrained molecules generally exhibit more favorable fluorescence characteristics than the unconstrained ones.

Based on this background, we have developed a new class of aromatic ring-fused BDP derivatives, boron–di(iso)indomethene (BDI) dyes (for general structure, see Scheme 1; the dyes prepared and investigated in this work are depicted in Scheme 2), by adopting the strategy of benzoporphyrin synthesis by means of a retro Diels–Alder reaction.[28] In the present paper, we elaborate the synthetic procedure and transfer it to the design and tuning of chemically addressable BDI derivatives that utilize charge-transfer processes for communication. Besides synthetic details, the molecular requirements, as can be deduced from X-ray structures, of the bicyclo-appended BDP (bc-BDP)[29] precursors as well as the BDI dyes are presented. The investigation of the precursor dyes, in particular, revealed some interesting mechanistic features of general BDP photochemistry. Owing to our interest in molecular switches and sensors and our experience with functionalized BDP dyes in this research area,[27,30] specific spectroscopic and redox features of the BDI derivatives have been introduced, by tuning the scaffold, to obtain a sodium-ion-responsive fluorescent sensor molecule.

Results and Discussion

Synthesis: The synthetic route for the preparation of compounds **4a–f** is depicted in Scheme 3. Ethyl 4,7-dihydro-4,7-

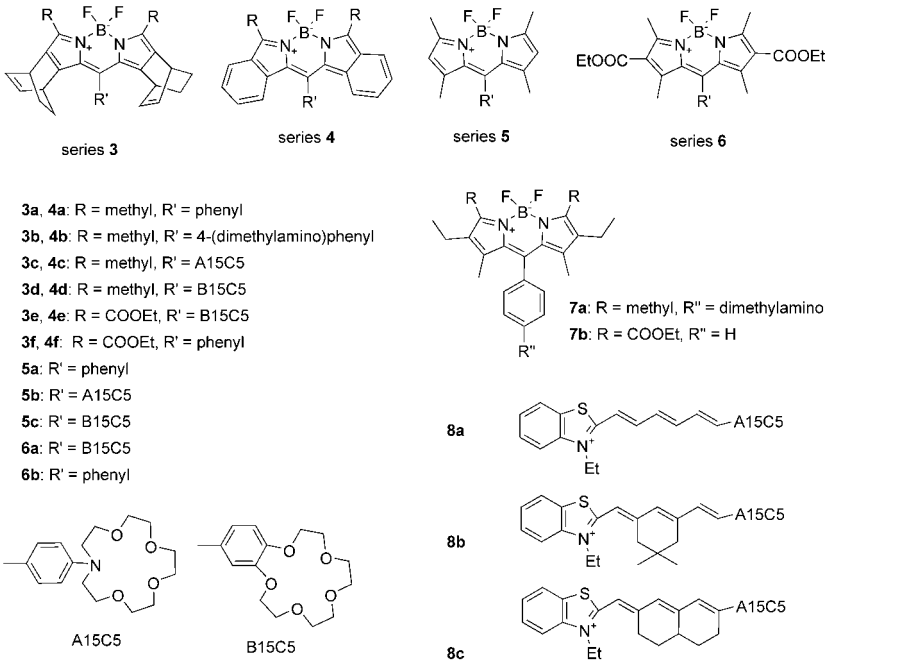

Scheme 2. Structures of the BDI compounds investigated (**4a–f**), the bicyclo-type precursors (**3a–f**), and some BDP (**5a–c**, **6a**,**b**, **7a**,**b**), as well as cyanine (**8a–c**) reference compounds.

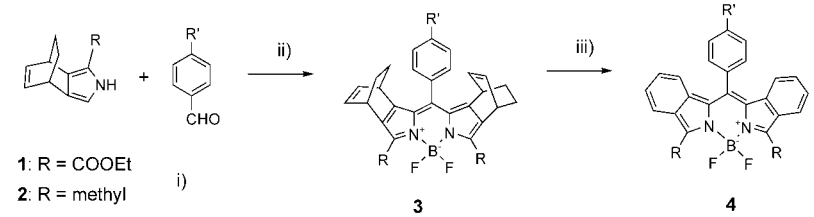

Scheme 3. Synthetic route to the preparation of compounds **4a–f**. Reagents and conditions: i) $LiAlH_4$, dry THF, reflux; ii) TFA, DDQ, EDIPA, $BF_3{\cdot}Et_2O$ in CH_2Cl_2; iii) 220 °C, 30 min.

ethano-2*H*-isoindole carboxylate (**1**) was prepared according to a method reported earlier by us[31] and was converted into 2-methyl-4,7-dihydro-4,7-ethano-2*H*-isoindole (**2**) by reduction with excess $LiAlH_4$ in dry THF under reflux for 2 h. Acid-catalyzed condensation of pyrroles **1** or **2** with various aldehydes followed by treatment with *N*-ethyl-*N*,*N*-diisopropylamine and $BF_3{\cdot}Et_2O$ yielded the bicyclo[2.2.2]octadiene-fused precursors **3a–f**. The latter were then quantitatively transferred into the aromatic ring-fused systems upon heating to 220 °C under reduced pressure (10 mmHg) for 30 min. We favored this strategy for several reasons:

1) Pyrroles fused with aromatic rings, namely isoindoles, are too unstable to be used directly for the preparation of such compounds.
2) Precursors **3a–f** can be prepared conveniently with satisfactory yields; they are also more stable in acidic or basic solutions and on silica gel than compounds **4a–f**.
3) Compounds **4a–f** are obtained via a retro Diels–Alder reaction and do not require further purification.

X-ray structure analysis: Single-crystal X-ray structures were obtained for compounds **3a**,**c–e**, **4a**, and **4d** and the basic features are listed in Table 1. The corresponding molecular configurations and conformations are shown in Figure 1. The average B–N bond length amounts to 1.549(10) Å, indicating that all the investigated compounds possess single B–N bonds. The average B–F bond is 1.380(10) Å and the average N-B-N and F-B-F angles are 107.3(6) and 110.6(14)°, respectively. These data indicate that the bond lengths and angles of the BF_2N_2 tetrahedron of the bc-BDP and BDI compounds of the present work are in good agreement with the corresponding values in the simpler analogues 4,4-difluoro-1,3,5,7,8-pentamethyl-3a.4a-diaza-4-bora-5-indacene,[32] 2,2-difluoro-1,3,4,6-tetramethyl-3-aza-1-azonia-2-borata-4,6-cyclohexadiene,[33] and 2,2-difluoro-4,6-dimethyl-1,3-di-*p*-toluyl-3-aza-1-azonia-2-boracyclohexa-4,6-dione.[34]

With regard to the prerequisites for the general spectroscopic features as well as the charge-transfer characteristics of such highly internally twisted composite chromophores, the conjugation and the planarity within the molecular fragment are important. The average bond length of N1–C4/N2–C5 is 1.353(10) Å, which indicates a pronounced double-bond character in contrast, for instance, to the average bond length of N1–C1/N2–C8, which is significantly longer (1.405(8) Å). Nonetheless, in all the compounds a strong π-electron delocalization is observed in **3a**,**c–e** within the central six-membered and both adjacent five-membered rings, and in **4a**,**d** within the whole ring system. This π-electron delocalization is interrupted between both B–N bonds.

For symmetry reasons, all ring atoms of **3a** and **4a** are exactly positioned within a plane. The atoms are on a mirror plane which coincides with that of the space group *Pnnm*. In **3c**,**d** and **4d**, the root-mean-square (rms) deviations of the ring atoms are 0.022 Å, 0.037 Å, and 0.012 Å, respectively, which also reveals a high planarity of the ring systems. In contrast, we found a certain distortion of the chromophore's planarity in **3e**, as manifested in a corresponding mean rms deviation of 0.195 Å. In this case, the ring system displays a "butterfly" conformation; the single "wings" consisting of two planes B1-N1-C1-C2-C3-C4-C9 and B1-N2-C5-C6-C7-

Table 1. Crystallographic data and details of the structure determinations of the compounds **3a**,**c**–**e** and **4a**,**d**.

	3a	**3c**	**3d**	**3e**	**4a**	**4d**
formula	$C_{29}H_{27}BF_2N_2$	$C_{39}H_{46}BF_2N_3O_4{\cdot}CH_2Cl_2$	$C_{37}H_{41}BF_2N_2O_5{\cdot}2\,CHCl_3$	$C_{41}H_{45}BF_2N_2O_9$	$C_{25}H_{19}BF_2N_2$	$C_{33}H_{33}BF_2N_2O_5$
M_r	452.34	754.55	881.26	758.62	396.23	586.42
T[K]	293(2)	298(2)	293(2)	298(2)	293(2)	293(2)
crystal system	orthorhombic	triclinic	orthorhombic	monoclinic	orthorhombic	triclinic
space group	*Pnnm*	$P\bar{1}$	*Pbca*	*Cc*	*Pnnm*	$P\bar{1}$
a[Å]	13.214(2)	11.938(2)	19.307(3)	22.653(7)	14.302(4)	8.2399(13)
b[Å]	18.342(3)	12.384(1)	18.032(3)	11.952(3)	20.467(5)	12.537(2)
c[Å]	9.732(2)	14.872(2)	23.990(4)	16.342(5)	6.909(2)	14.634(2)
α[°]	90	74.083(9)	90	90	90	70.993(2)
β[°]	90	69.963(10)	90	124.563(5)	90	89.259(4)
γ[°]	90	70.100(10)	90	90	90	85.554(3)
V[Å^3]	2358.9(6)	1911(4)	8352(3)	3643(1)	2022.5(9)	1424.9(4)
Z	4	2	8	4	4	2
ρ_{calcd}[g cm^{-3}]	1.274	1.311	1.402	1.383	1.301	1.367
μ[mm^{-1}]	0.085	0.224	0.465	0.103	0.089	0.100
F(000)	952	796	3648	1600	824	616
crystal size [mm]	0.20×0.22×0.28	0.20×0.40×0.60	0.32×0.38×0.42	0.10×0.15×0.30	0.05×0.10×0.25	0.04×0.11×0.23
θ_{max}[°]	28.5	27.5	27.5	27.5	25.0	25.0
index ranges	$-18\le h\le 16$	$-15\le h\le 14$	$-25\le h\le 24$	$-29\le h\le 25$	$-18\le h\le 19$	$-11\le h\le 10$
	$-26\le k\le 23$	$-16\le k\le 0$	$-24\le k\le 11$	$-15\le k\le 15$	$-29\le k\le 24$	$-17\le k\le 16$
	$-13\le l\le 7$	$-19\le l\le 18$	$-34\le l\le 31$	$-18\le l\le 21$	$-9\le l\le 7$	$-12\le l\le 20$
unique reflections	3136	9185	9579	6785	1937	4942
reflections observed [$I>2\sigma(I)$]	1948	4369	5175	5194	1295	2370
parameters	250	486	649	493	222	389
$R1$ (on F) [$I>2\sigma(I)$]	0.0452	0.0650	0.0672	0.0772	0.0448	0.0591
$wR2$(on F^2)	0.1311	0.1650	0.2002	0.1760	0.1090	0.1565
largest diff. peak/hole [eÅ^{-3}]	0.234/−0.156	0.47/−0.62	0.637/−0.501	0.78/−0.38	0.174/−0.235	0.434/−0.162

C9. The dihedral angle between both planes is 14.3(9)°. The significant deviation from coplanarity is most probably caused by steric hindrances between both fluorine atoms and the oxygen atoms O7 and O8 of the ester groups (Figure 1).

In **3c**–**e**, the double bonds C11=C12 and C15=C16 are on opposite sides of the molecular plane; that is, the ring systems contain approximately a twofold axis passing through B1 and C9. This in turn leads to the conclusion that in the synthesis, molecular parts with the same absolute configuration were fused. This should also be true for compound **3a**. However, the crystal structure of **3a** is disordered as the mirror plane of the space group *Pnnm* passing through the atoms of the fused rings is fulfilled only statistically.

With respect to the methene-appended crown-substituted phenyl moieties in **3c**–**e** and **4d**, the important structural features of the heteroatom fused to the phenyl's *para* (and *meta*, in the case of the benzocrowns) position can be rationalized as follows: in **3c**, the nitrogen atom N3 has a sp^2 hybridization state, because the sum of the bond angles equals 359.7°. Moreover, the bond length N3−C21 = 1.387(3) Å is substantially shortened with respect to the alkyl amino bonds N3−C26 = 1.450(5) Å and N3−C35 = 1.452(4) Å. In **3d**,**e** and **4d**, the distances between the crown O atoms and the *p*/*m*-phenyl C atoms are also significantly shorter than the other ether-type O−C bonds within the crown. The average value for the first type of bond is 1.365(5) Å, and the ether bonds show an average length of 1.419(12) Å.

For symmetry reasons, the phenyl rings C18-C19-C20-C21-C20′-C19′ are positioned exactly perpendicularly to the ring system in **3a** and **4a**. For the other molecules, the conformation may be described by the dihedral angles between the planes of the chromophore E1 (B1, N1, C1–C9), the methene-appended phenyl ring E2, and the crown's non-hydrogen atoms E3. Interestingly, as can be seen from Table 2, the expected virtually orthogonal conformation is only found for the BDI derivative **4d**. However, **3c**–**e** exhibit an internal twist of the E1–E2 planes that is rather close to biaryl derivatives, such as 9,10-diphenylanthracene (θ = 67°)[35] or 10-methyl-9-*p*-A15C5-phenylacridinium perchlorate (θ = 57°),[36] which do not carry sterically demanding substituents at positions close to the interannular bond.

Figure 2 shows the molecular packing in the crystal structures of **4a** and **4d**. In **4a**, strong π–π electron interactions exist between *n*-glide-plane-related molecules to form infinite layers perpendicular to the *b* axis in the crystal. The plane-to-plane distance is 3.45 Å. In the crystal of **4d** (Figure 2), strong π–π electron interactions are found between the molecular ring systems of molecules related by a translation in the *x* direction by a_o to form infinite stacks. The plane-to-plane distance here is 3.49 Å. In addition to these interactions, relatively strong van der Waals contacts (shorter than 3.5 Å) between adjacent crown moieties related by a center of symmetry are found for this molecule. For sterical reasons, comparable stacking interactions are not possible in the dyes of the **3** series.

Absorption and fluorescence spectroscopy of 3a–d and 4a–d: The absorption and emission spectra of the bc-BDP and BDI dyes carrying only alkyl substituents on the (π-extended) core are of similar shape to those of the classical BDP dyes. In absorption, both series show narrow spectra with two maxima, the global maximum appearing at $\lambda = 527 \pm 3$ nm for **3a**–**d** and at 598 ± 3 nm in the case of **4a**–**d**, irre-

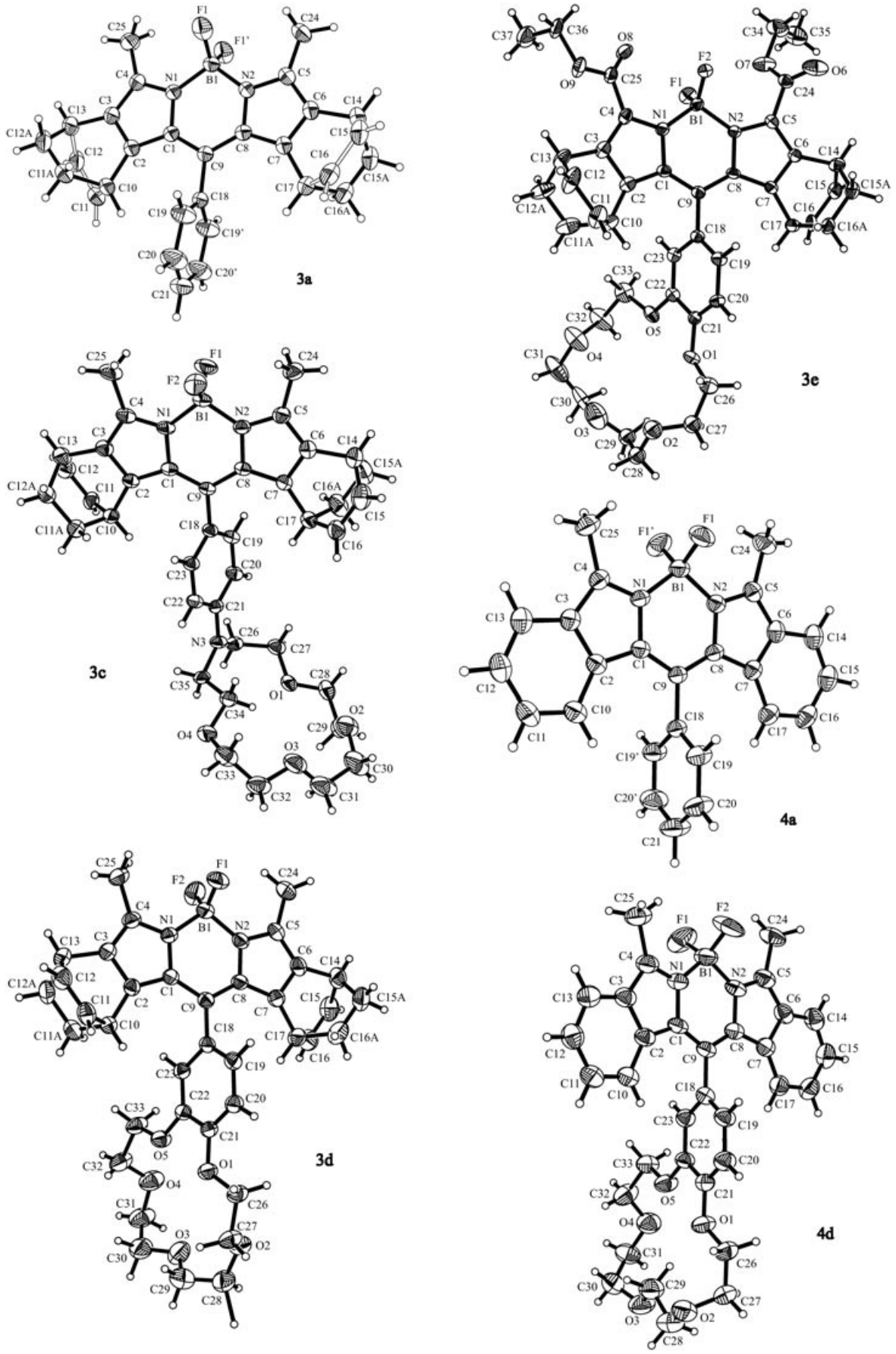

Figure 1. ORTEP plots of **3a**, **3c–3e**, **4a**, and **4d**. For better clarity, only ordered molecules are shown; in the case of **3c** and **3d**, the CH_2Cl_2 and $CHCl_3$ solvent molecules, respectively, were omitted.

Table 2. Dihedral angles [°] of the molecular planes as defined in the text.

	θ_{E1-E2}	θ_{E2-E3}
3c	65.0(1)	60.3(1)
3d	67.6(1)	16.2(1)
3e	67.9(1)	19.9(2)
4d	80.9(1)	4.9(1)

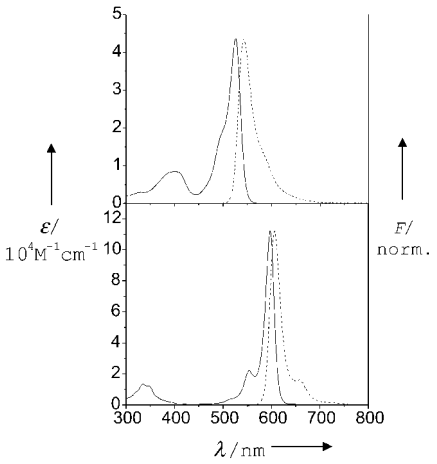

Figure 3. Absorption (——) and emission (-----) spectra of **3a** (upper part, excited at 495 nm) and **4a** (lower part, excited at 553 nm) in acetonitrile.

spective of the solvent employed. The second maxima, or shoulders on the high-energy side, are centered at $\lambda \approx 496$ and 555 nm, respectively (Figure 3). In addition, a considerably weaker, broad absorption band is found at ≈ 400 nm for the bicyclo compounds (Figure 3, upper part), and its position is also not significantly affected by solvent polarity. Analysis of the molecular orbitals (MOs) obtained in 1SCF calculations for the AM1-optimized ground state geometries of **3a** and **4a** reveals that the HOMO–LUMO transition shows typical cyanine features (Figure S1, Supporting Information). Both MOs are delocalized along the polymethinic chain of the BDP and BDI core with alternating patterns and show a large orbital overlap, and are thus strongly allowed in both cases. Besides this oscillator-strong transition, a second lowest transition in the 350–400 nm range with a ≈ 5 times reduced oscillator strength is only found for **3a**. The molecular orbitals predominantly involved here are the HOMO−1/−2 and the LUMO, the two former are now approximately equally localized on the polymethinic BDP core and the bicyclo fragments. For **4a**, the second lowest transition is even less intensive and is only found at higher energies. Again, it is located on the entire BDI core. We thus attribute the broader and weaker absorption band in the **3** series to the $S_2 \leftarrow S_0$ transition, which partly involves the bicyclo skeleton. Within the **3** and the **4** series, the variation of the substituent in the 14-position has no influence on these two transitions. The typical weak aniline-type absorption band is found at ≈ 270 nm only in the case of the 14-alkylanilino derivatives. In relation to the twist angles θ_{E1-E2} between the two biarylic molecular fragments, as found in the X-ray analyses, the subunits seem to be entirely electronically decoupled in the dyes in liquid solutions. Packing effects most probably account for $\theta_{E1-E2} \sim 70°$ of some of the bc-BDP derivatives in the crystal.

To obtain further information on the influence of the solvent on the lowest energy transition, the intense $S_1 \leftarrow S_0$ bands were converted to the energy scale and spectrally deconvoluted by means of a progression of Gaussian functions (Section S2 in the Supporting Information). For both series of dyes, the full width at half maximum (fwhm) of the absorption bands only increase slightly as a function of the po-

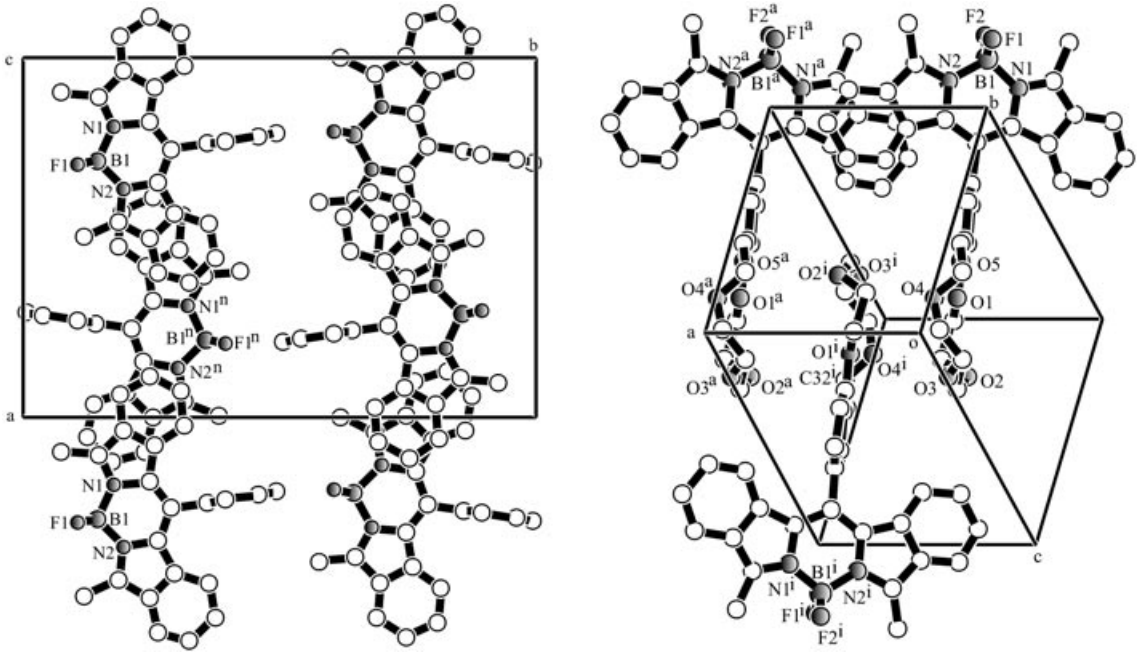

Figure 2. Molecular packing in the crystal structure of **4a** (left) and **4d** (right).

larity of the solvent (Table 3, and Tables S1 and S2 in the Supporting Information), which is presumably related to the high rigidity and weak dipolar nature of the chromophores.[37] At the same time, it is evident that the fwhm of **4a–d** are distinctly smaller than those of **3a–d**. In both cases, the nature of the substituent in the 14-position has again virtually no effect on these properties (Table 3, and Tables S1 and S2 in the Supporting Information; note that the 14-position of the tetrahydrobis(ethano)diisoindoles or bc-BDPs corresponds to the 8-position of the classical BDPs). A similar reduction in bandwidth is found for the cyanine reference compounds **8a–c**[38] with increasing degree of bridging in the polymethine chain; that is, fwhm = 970, 780, and 710 cm^{-1} for **8a–c**, respectively. In both cases, the reduction in the degree of flexibility—by bridging the bonds in the **8** series and by increasing the planar aromatic skeleton for **4** versus **3**—diminishes the degrees of vibrational freedom. Moreover, the results of the spectral analysis support these assumptions. The fits yield equidistant spacings for the maxima of the single subbands; this freely fitted parameter was calculated as 710 ± 40 cm^{-1} for **3a–d** and 460 ± 30 cm^{-1} for **4a–d**. As can be deduced from Figure S4 (in the Supporting Information), the molecular C–C frame vibration of ≈ 1300 cm^{-1}, which is typical for cyanine dyes, is also found for the present compound families. On the other hand, the more expanded and more rigid BDI chromophoric system is also reflected by the considerably higher extinction coefficients of the dyes of the **4** series relative to the bc-BDPs. A representative couple here is **4d** with $\varepsilon_{598} = 112\,760 \pm 2250$ $cm^{-1}\,M^{-1}$ and **3d** with $\varepsilon_{526} = 46\,160 \pm 500$ $cm^{-1}\,M^{-1}$ in acetonitrile, while the oscillator strengths of the entire transition differ only by a factor of 1.5 (see also Figure 3 for comparison).

As can be deduced from Figure 3, excitation of the bc-BDPs and BDIs yields fluorescence spectra with a mirror-image shape. The Stokes shifts are generally larger for the **3** series than those of dyes **4a–d** (Table 3), and the fluorescence excitation spectra match the absorption spectra in all the cases. While the BDP dyes with the core not fully alkylated show emission maxima at $\lambda = 500$–510 nm,[30a–c] the fluorescence bands of **3a–d** are found at 542 ± 2 nm, which is comparable to those of the tetramethyldiethyl-(8-phenyl)-substituted derivatives.[30d] The spectra of **4a–d** are further red-shifted, and are centered at 606 ± 2 nm. Again, the band positions do not show any particular trend as a function of solvent polarity. These features suggest that emission occurs from the weakly polar, relaxed Franck–Condon excited state of the dyes. The use of a similar fitting procedure as for the absorption spectra showed the same trends of slightly narrowing bands with reduced solvent polarity. In general, the fwhm and the spacings $\Delta\tilde{\nu}$ of the absorption and emission bands agree rather well, and support the classification of the bc-BDP and BDI chromophores as polymethines.[39] However, the agreement is better for the highly conjugated dyes (e.g., $\Delta\tilde{\nu} = 460$ vs 480 cm^{-1} for absorption vs emission for the **4** series, but 710 vs 810 cm^{-1} for the **3** series), which stresses the influence of the rigidity of the BDI chromophore. In addition to the decrease in fwhm, the Stokes shift gradually decreases for a certain dye on going from an acetonitrile to a hexane environment, reflecting the influence of the solvation capability of the solvents on such types of highly delocalized and weakly dipolar chromophores. Dual fluorescence as has been observed for several 8-*p*-aminophenyl-substituted classical BDP dyes (e.g. **5b**; as well as other dyes[30a,b]) could be reliably detected in the present case only for **3b** and **3c** in THF; the maximum of the broad

Table 3. Selected spectroscopic data of **3a–d** and **4a–d** in hexane and acetonitrile. For comprehensive solvent-dependent data, see Tables S1 and S2 in the Supporting Information.

	Solvent	λ_{abs} [nm]	$fwhm_{abs}$ [cm^{-1}][a]	λ_{em} [nm]	$fwhm_{em}$ [cm^{-1}][a]	$\Delta\tilde{\nu}_{abs\text{-}em}$ [cm^{-1}][b]	Φ_f[c]	τ_f [ns]	k_r [10^8 s^{-1}]	k_{nr} [10^8 s^{-1}]
3a	hexane	529	754	544	848	484	0.90	5.96	1.5	0.2
	MeCN	526	812	543	907	563	0.81	6.18	1.3	0.3
3b	hexane	527	718	540	808	427	0.93	5.51	1.7	0.1
	THF[d]	527	796	544	984	624	0.16	0.03	[e]	[e]
	MeCN[f]	524	824	542	980	687	< 0.001[g]	< 0.003	n.d.[h]	n.d.[h]
3c	hexane	527	742	539	791	416	0.80	5.53	1.4	0.4
	MeCN[f]	524	841	543	1024	728	0.0009	0.01	1.5	1660
3d	hexane	529	746	542	777	434	0.90	6.59	1.4	0.1
	MeCN	526	784	541	827	503	0.84	6.45	1.3	0.2
4a	hexane	599	440	605	530	176	0.91	5.71	1.6	0.2
	MeCN	597	582	606	593	241	0.87	5.63	1.5	0.2
4b	hexane	599	450	605	527	155	0.90	5.65	1.6	0.2
	MeCN	597	532	605	577	222	0.022	0.19	1.2	51
4c	hexane	599	487	605	509	143	0.74	5.52	1.3	0.5
	MeCN	598	516	606	560	210	0.093	0.70	1.3	13
4d	hexane	n.d.[i]	n.d.[i]	605	511	n.d.[i]	0.78	5.45	1.4	0.4
	MeCN	598	537	607	605	252	0.86	5.66	1.5	0.2

[a] Obtained from the data treatment and fitting procedure described in the text and Supporting Information, fwhm ± 10 cm^{-1} (for **3** series) and ± 5 cm^{-1} (for **4** series). [b] Obtained as described in the Experimental Section. [c] Fluorescence quantum yield in the region of LE emission; after deconvolution in case of dual emission. [d] Features of the dominant species in the region of the typical BDP or LE emission; CT emission band characteristics are $\lambda = 674$ nm, fwhm = 6900 cm^{-1}, $\Phi_f = 0.022$. The decays are biexponential over the entire emission spectrum with a second decay time of $\tau_f = 3.39$ ns. [e] See discussion and data in the text for more details. [f] No CT fluorescence could be detected. [g] Could not be reliably determined. [h] Not determined. [i] Not determined due to too low solubility.

and red-shifted charge-transfer emission appearing at $\lambda =$ 674 and 641 nm, respectively. The time-resolved fluorescence measurements gave further evidence for this observation, vide infra.

The similarity of the nature of the absorbing and the emitting state can be deduced from an analysis of the transition dipole moments of absorption and emission, M_{abs} and M_{em}, by way of the radiative rate constants observed experimentally [k_r, Eq. (1)] and calculated from the absorption spectra [k_r^{calcd}, Eq. (2)]. Here, n is the refractive index of the solvent, c_0 the speed of light in vacuum, and h and N_A are the Planck and the Avogadro constants, respectively.[40]

$$k_r = \frac{\Phi_f}{\tau_f} = \frac{64\pi^4}{3h} n^3 \tilde{\nu}_{em}^3 |M_{em}|^2 \quad (1)$$

$$k_r^{calcd} = \frac{64\pi^4}{3h} n^3 \tilde{\nu}_{em}^3 |M_{abs}|^2$$
$$|M_{abs}|^2 = \frac{3hc_0 \ln 10}{8\pi^3 N_A n} \int_{band} \frac{\varepsilon(\tilde{\nu}_{abs}) d\tilde{\nu}_{abs}}{\tilde{\nu}_{abs}} \quad (2)$$

The ratios $k_r/k_r^{calcd} = 1.00 \pm 0.05$, obtained for **3d** and **4d** in acetonitrile and dibutyl ether, stress the previous interpretation of the data that the differences in conformation involved in the absorption and emission processes seem to be rather small and solvent-independent.

The fluorescence quantum yields (Φ_f) are always high in solvents of rather low polarity, such as diethyl ether or hexane (Table 3 and Tables S1 and S2 in the Supporting Information). For the 14-phenyl-substituted derivatives **3a** and **4a**, these features are unchanged upon increasing the polarity of the solvent. However, an inspection of the respective data of the 14-dimethylanilino-substituted dyes **3b** and **4b** reveals that the fluorescence is quenched with increasing solvent polarity. A similar trend is registered for the fluorescence lifetimes. Except for **3b** in THF (and **3c**, see Table S1 in the Supporting Information), monoexponential decays are found for all dyes (Table 3 and Tables S1 and S2 in the Supporting Information). Accordingly, the rate constants of fluorescence k_r[41] show a minor solvatokinetic modulation for **3a–d** and **4a–d**. The concomitant, distinctly more pronounced increase in the nonradiative rate constant k_{nr} thus suggests that not only does **3b** behave similarly to its classical BDP analogue with less sterically demanding substituents,[30a] but also an addressable and analytically potentially valuable deactivation process can be installed in the BDI derivatives. Here, two different regions are noticed in a plot of k_{nr} as a function of the solvent polarity; this suggests that the quenching process is activated in solvents more polar than THF (Figure 4). Consequently, when equipping the bc-BDP and BDI core with a phenyl-A15C5 substituent, these features are preserved and dyes **3c** and **4c** also exhibit charge- or electron-transfer-type quenching of the emission. As has been discussed above, the electron-donating nitrogen atom in the 14-anilino moiety of **3c** is sp^2 hybridized and thus readily feeds its electrons into the 14-phenyl ring. The distance between these "virtually decoupled" ET partners is at a minimum. It is interesting to note that the long wavelength dyes of the **4** series, which are equipped with a strong anilino-type donor in the 14-position, do not show any dual fluorescence. Apparently, as has been found for the distyryl-substituted BDP chromophore that also emits at >600 nm,[27b] the excited-state charge-transfer process leads to the formation of a nonemissive CT state in the BDI case, too. Furthermore, because the flexibility in **4b**,**c** is reduced to a minimum, it seems reasonable to assume that an energetic limit exists for the charge-recombination fluorescence from strongly forbidden CT transitions, which is located somewhere between 2.07 and 2.48 eV for the present type of dye. At energies below this threshold, deactivation of such highly twisted excited-state species seems to be entirely radiationless. On the other hand, **3d** as well as **4d**, which carries the less electron-donating benzocrown unit, show a high fluorescence emission that is independent of solvent polarity.

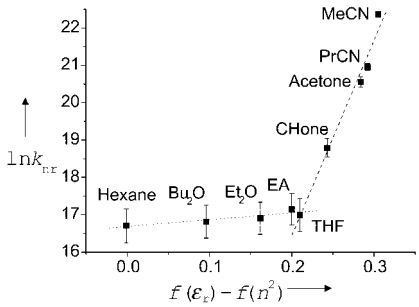

Figure 4. Plot of the nonradiative rate constant vs solvent polarity for **4b** (data from Table S2 in the Supporting Information, EA = ethyl acetate, CHone = cyclohexanone, PrCN = propionitrile). The two different regions are indicated by a fit (——) and a trendline (·····), the latter as a guide to the eye.

Analysis of the dual fluorescence features of **3b** in THF, according to a procedure described in more detail in reference [30a], revealed the following characteristics: the ratio of charge transfer to BDP-localized (or locally excited, LE) fluorescence $\Phi_f(CT)/\Phi_f(LE) = 0.14$. This value is distinctly lower than $\Phi_f(CT)/\Phi_f(LE) = 2$ of the all core-alkylated model dye **7a** in THF.[42] In combination with the overall stronger fluorescence of **3b** in this solvent, $\Phi_f = 0.18$ versus 0.03[42] for **7a**, this suggests that CT state formation is less efficient in the sterically more hindered dye (for the respective, virtually identical redox data and electron-transfer driving forces, see below). Following the procedure in reference [30a], the excited-state reaction dynamics of **3b** in THF are determined to $k_{LC} = 31.9 \times 10^9\ s^{-1}$, $k_{CL} = 3.6 \times 10^9\ s^{-1}$, and $(\tau_0^{CT})^{-1} = 0.31 \times 10^9\ s^{-1}$ (for parameters, see Scheme 4 and reference [43]). The ratio of $k_f^{CT}/k_f^{LE} = 0.02$ indicates

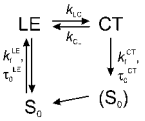

Scheme 4. Generalized kinetic scheme for the charge-transfer process in **3b** in THF. Where k are the respective rate constants and τ_0 the intrinsic lifetimes of the LE and CT states. The CT-type ground state is highly unstable and relaxes immediately to the initial ground state.

that fluorescence from the perpendicular state is forbidden, and the ratio of the excited-state reaction rate constants $k_{LC}/k_{CL}=8.9$ stresses the observation that the CT state is still efficiently populated, yet the reaction is less strong than in the simpler alkylated BDP analogues.

To obtain a better insight into the nature of the quenching process in the alkylanilino-substituted derivatives and its dependence on molecular motions, absorption as well as steady-state and time-resolved fluorescence measurements were carried out with **3b** in ethanol as a function of temperature, as well as with **3a** and **4a**,**b** in ethanol at 299 and 77 K. In all cases, the typical spectroscopic features of the bc-BDP and BDI dyes are observed; that is, the narrow absorption and emission bands of mirror-image shape and monoexponential decay kinetics.[44,45] Upon reducing the temperature, the width of the spectral bands is further reduced, the vibronic structure more pronounced, and the maxima show slight red-shifts below the freezing point of the solvent. Concomitantly, the fluorescence quantum yields and lifetimes of dyes **4b** and **3b** increase significantly with decreasing temperature, while those of **3a** and **4a** show a much less pronounced increase. For instance, τ_f of **3a** and **4a** change from 6.44 and 5.53 to 7.37 and 8.52 ns, respectively, upon cooling a solution of the dye in ethanol from 299 K to 77 K. The corresponding data of the 14-donor-substituted derivatives were determined to 0.09 and 6.06 ns for **3b** and 2.48 and 5.09 ns for **4b** at 299 and 77 K, respectively. Following the arrest of the CT process in **3b** by gradually reducing the temperature revealed that the photophysical parameters are largely constant at temperatures below the glass temperature of ethanol ($T_g^{EtOH}=158$ K). This suggests that the quenching process is blocked below T_g. Furthermore, analysis of the temperature-dependent emission data above T_g in terms of the Arrhenius equation [Eq. (3)] yielded a linear correlation for a plot of $\ln k_{nr}$ versus T^{-1} and allowed the calculation of an activation barrier of 7.9 kJ mol^{-1} for the nonradiative processes in **3b** in ethanol.[46] On the other hand, k_r does not show a distinct temperature dependence with values of $1.5(\pm 0.3)\times 10^8$ s^{-1} over the entire temperature range studied. This behavior points to a predominantly viscosity-controlled quenching process that is active in the 14-alkylaminophenyl derivatives.

$$\ln k = \ln A - E_A/RT \qquad (3)$$

An analysis of the fluorescence anisotropy data of **3a**,**b** and **4a**,**b** in propylene glycol at 223 K provided further information on the orientation of absorption and emission dipoles within such molecules. Figure 5 reveals that r values close to 0.4 are found for **3a**, **4a**, and **4b** in the region of the BDP and BDI bands.[47] Thus, the dipoles of both transitions are highly colinear, and oriented along the long axis of the respective core. For **3a**,**b**, r decreases in the region of the $S_2 \leftarrow S_0$ transition between 350–400 nm. This is consistent with the involvement of the bicyclo rings, which induce a symmetry distortion. The higher transitions (<400 nm) in **4a**,**b** are partly mixed and involve various molecular orbitals localized asymmetrically on the BDI fragment, entailing r values between 0.1–0.2 with dipole differences up to ≈45°.

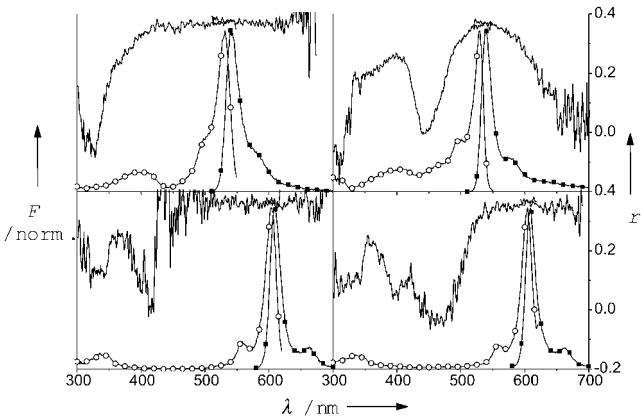

Figure 5. Fluorescence excitation (○) and emission (●) spectra of **3a** (upper left), **3b** (upper right), **4a** (lower left), and **4b** (lower right) in propylene glycol at 223 K. The corresponding anisotropies are included.

The reduction in r to ≈0 around 440 nm for **3b** and 470 nm for **4b** is probably related to oscillator-weak transitions involving the *meso*-substituent. Moreover, in the case of **3b**, the decrease of r on the low-energy side of the BDP emission and at ≈500 nm on the high-energy side of the excitation bands suggests some admixing of other transitions and remains unclear at the present stage of investigation. This fact along with the peculiar CT features of **3b** indicate that further experiments are necessary to obtain a more detailed picture of the deactivation processes in the *meso*-donor-substituted precursors of the BDI dyes.

Cation-induced chemical switching features of 3c and 4c in MeCN and of 3d and 4d in MeOH: Whereas the absence of a quenching process in **3d** might be rationalized in terms of the similar behavior of **5c**,[30c] the immunity of **4d** against the activation of an electron-transfer process has a strong impact on the design of efficient BDP-type fluorescent switches for the red spectral range. Before we attempt to access the underlying energetics and thus a means of how to improve the BDI chromophore, exemplary cation-induced switching features of the crowned dyes **3c**,**d** and **4c**,**d** will be briefly presented.

The cation selectivities of the A15C5-substituted dyes are similar to those found previously for many other such fluoroionophores,[48] and thus we will concentrate on protons and particular Group I and Group II metal ions here. The quenched fluorescence of **3c** and **4c** can be entirely revived by protonation. This yields $\Phi_f=0.72$ and $\tau_f=6.01$ ns for **3c**-H^+ and $\Phi_f=0.91$ and $\tau_f=5.58$ ns for **4c**-H^+ in MeCN.[49] Accordingly, upon binding of alkali and alkaline-earth metal ions to the A15C5 unit, the latter's electron-donating ability is also reduced and thus the CT process is interrupted. For instance, **3c**-Na^+ shows a high fluorescence enhancement factor (FEF) of 41. Very similar to the characteristics of **5b**-Na^+,[30a] this pair also forms two different, spectrally undistinguishable complex species, as manifested in a biexponential decay of the typical BDP fluorescence ($\tau_f=0.35$ and 2.72 ns, amplitude ratio = 1.02; see reference [30a] for a more detailed discussion). In contrast, all the alkali and al-

kaline-earth metal ion complexes of **4c** display only single exponential decays, ranging for example, from $\tau_f = 4.46$ ns for **4c**-K^+ to 5.75 ns for **4c**-Ca^{2+}. The corresponding fluorescence quantum yields are generally high with an average of 0.7 for the monovalent and 0.85 for the divalent cation complexes. This simultaneous increase in fluorescence quantum yield and lifetime signifies that the k_r of the complexes are rather similar to those of the unbound dyes and only the k_{nr} are reduced; the quenching process is switched off. Owing to the higher quantum yield of **4c** in the unbound state, the FEF between 7.5 and 9.5 are lower for the red-emitting dye. Moreover, the bulkiness of the BDI core with its annelated phenyl rings, which point in the direction of the receptor unit, seems to shift the equilibrium of different complex conformers to one form only, thus yielding monoexponential decays.

The spectral properties of the complexes are rather similar to those of the free dyes. For **3b**-H^+ as well as **3c**-M^{n+}, the absorption and fluorescence spectra are slightly red-shifted (e.g. to 528/545 and 531/551 nm for **3b**-H^+ and **3c**-Ca^{2+}, respectively), and the widths are slightly larger. The mirror-image relationship is also found. Since upon excitation, the electron density is increased at the 14-position of the bc-BDP core in the **3** series (see Section S1 in the Supporting Information), the red-shift upon protonation or cation binding is conceivable with the change from a donor to an acceptor moiety in this position. All these effects are less pronounced in the case of **4b**,**c** (spectral red-shifts of 1 or 2 nm, Figure 6), in which the change in electron density at the 14-position, obtained from the quantum chemical calculations, is less pronounced. The complex stoichiometries determined from titrations are 1:1. However, whereas **4c** and Na^+ or Ca^{2+} show complex stability constants that agree well with those of **5b**, complex formation is evidently hampered by the bulky bicyclo groups in **3c**, resulting in lower $\log K$ for both Na^+ and Ca^{2+} in MeCN (see Table 4).

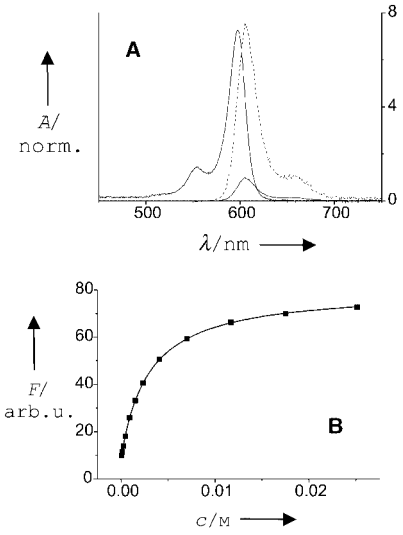

Figure 6. A) Absorption and emission spectra of **4c** (——) and **4c**-Na^+ (·····) in acetonitrile. The absorption band of the complex overlaps strongly and is omitted for clarity. B) Corresponding, representative titration curve ($c_{\mathbf{4c}} = 1.2 \times 10^{-6}$ M).

Table 4. Selected complex stability data of the sensor molecules investigated.

Complex	Solvent	$\log K$
3c-Na^+	MeCN	1.95
3c-Ca^{2+}	MeCN	3.95
4c-Na^+	MeCN	2.53
4c-Ca^{2+}	MeCN	4.56
5b-Na^+	MeCN	2.20
5b-Ca^{2+}	MeCN	4.40
3e-Na^+	MeOH	2.50
4e-Na^+	MeOH	2.35

Evidently, **3c** and **4c** with an A15C5 unit suffer from a low selectivity and this nitrogen-atom-containing receptor is not very suitable for selectively targeting a biologically important alkali metal ion, such as sodium. The use of a benzocrown instead would improve the chances of obtaining selective Na^+ fluoroionophores. However, as already mentioned above, **3d** and **4d** show a strong fluorescence in solvents from hexane to methanol and, thus, these molecules remained spectroscopically silent toward Na^+ in methanol. Therefore, further modification of the BDI chromophore became necessary.

Electrochemical properties of 3a–d and 4a–d: Before setting out to enhance the BDI core, a detailed analysis of the electron-transfer features of the dyes presented so far is indispensable. Thus, the redox properties of the compounds were studied by cyclic voltammetry in 0.1 M TBAP in acetonitrile. The electrochemical data and electron-transfer parameters of **3a–d**, **4a–d**, and the reference compounds **5a–c**, and **7a** are given in Table 5. Compound **3a** displays a reversible one-electron reduction wave at the same potential ($E^{red}_{1/2} = -1570$ mV vs Fc^+/Fc) and a reversible oxidation wave at a slightly less positive potential ($E^{ox}_{1/2} = 670$ mV) than the conventional BDP model dye **5a**. The reduction potentials of **3b–d** are slightly negatively shifted into the range from −1595 to −1640 mV, and a second oxidation wave ap-

Table 5. Redox potentials and electron-transfer data of compounds **3a–d**, **4a–d** and various model compounds (in CH_3CN, $c = 10^{-3}$ M, 0.1 M TBAP, $v = 250$ mV s^{-1}).[a]

	$E^{red}_{1/2}$ [mV]	$E^{ox}_{1/2}$ [mV][b]	$E^{ox}_{1/2}$ [mV][c]	E_{00} [eV]	ΔG_{ET} [eV]
3a	−1570	670	–	2.36	–
3b	−1640	740	540	2.37	−0.3
3c	−1640	730	570	2.37	−0.1
3d	−1595	665	1150[d]	2.36	0.3
4a	−1530	330	–	2.07	-
4b	−1590	290	630[e]	2.08	0.0
4c	−1600	310[e]	700[e]	2.07	0.1
4d	−1565	325	1150[d]	2.07	0.5
5a[f]	−1560	760	–	2.49	–
5b[f]	−1600	840	570	2.50	−0.4
5c[g]	−1575	750	1150[d]	2.49	0.1
7a[f]	−1686	700	512	2.39	−0.3

[a] Referenced against Fc^+/Fc. [b] BDI or bc-BDP chromophore. [c] Group in the 14- or 8-position. [d] Value of dimethoxybenzene. [e] Quasireversible. [f] Redox data taken from reference [42]. [g] Redox data taken from reference [30c].

peared that is attributed to the oxidation of the 4-nitrogen substituents on the *meso* aromatic ring in compounds **3b** and **3c**. The oxidation potential for the benzocrown moiety in **3d** is much higher and cannot be detected. To calculate the driving force ΔG_{ET} of the excited-state electron-transfer reaction according to Equation (4), we thus take the tabulated value of dimethoxybenzene ($E^{ox}_{1/2} = 1150$ mV vs Fc^+/Fc).[30c] A comparison of this value with those given for the amino substituents in Table 5 indicates that the benzocrown group is a considerably weaker donor than the anilino or azacrown units.

$$-\Delta G_{ET} = \Delta E_{00} - IP_D + EA_A + E_C \quad (4)$$

In Equation (4) ΔE_{00} is the zero–zero transition energy of the excited donor–acceptor pair, IP_D is the ionization potential of the donor, EA_A is the electron affinity of the acceptor, and E_C is the Coulomb stabilization energy of the radical ion pair $D^{\bullet+}-A^{\bullet-}$, taken to 0.1 eV.[30c] As can be deduced from the data of **3b**,**c**, **5b**, and **7a** in Table 5, the driving forces for these anilino-substituted BDPs are rather similar and largely correlate with the fluorescence deactivation parameters for a single series.

Compared with **3a**–**d**, the reduction potentials of **4a**–**d** are only slightly shifted to more positive values, for example, **4a** shows a reversible one-electron reduction at = −1530 mV. However, their oxidation potentials are considerably negatively shifted (e.g. to 330 mV for **4a**), approximately ten times more than the reduction potentials. These findings indicate that fusion of the benzene rings strongly increases the HOMO energy level, while the LUMO energy levels are virtually unaffected.[50] As a consequence, the HOMO–LUMO separation in **4a**–**d** is narrowed. In addition, a second oxidation wave appeared for **4b**,**c** that is attributed to the oxidation of the nitrogen donor atom. The oxidation of the receptor group in the benzocrown derivative **4d** is again much higher and could not be detected under the experimental conditions used. From the ΔG_{ET} data in Table 5, it is apparent that the values for **4b**,**c** are distinctly higher than those of the corresponding bc-BDPs; this reflects the generally higher fluorescence emission of the 14-anilino BDIs in highly polar solvents.

Tuning the BDI chromophore toward 4e,f: On the basis of previous design considerations,[30c] the introduction of electron-withdrawing substitutents, such as ester groups, to the pyrro- or indomethene core seems to provide a means to activate a redox-based quenching process in otherwise silent ensembles. Accordingly, we synthesized **4e**,**f** via the precursors **3e**,**f**, vide supra. As is evident from Table 6, the introduction of the ester groups indeed causes the redox potentials to dramatically shift to the positive. Moreover, in comparison to our previous example, the 300 mV shift of the reduction and oxidation potentials of **5c** with respect to **6a**, the shifts in the bc-BDP system are almost twice as large. For instance, the reduction potential of **3f** is 630 mV less negative, and the oxidation potential is 540 mV more positive than that of **3a**. Even more favorably, such dramatic effects are also observed in the more conjugated **4f** (690 mV positive shift for reduction and 490 mV positive shift for oxidation) and **4e** (695 mV positive shift for reduction and 425 mV positive shift for oxidation) with respect to **4a** and **4d**. Accordingly, the HOMO–LUMO energy gaps of the present dyes are narrowed even further. With regard to the electron-transfer driving force, both **3e** and **4e** should now show the favorable quenched fluorescence in the unbound state.

Table 6. Redox potentials and electron-transfer data of compounds **3e**,**f**, **4e**,**f** and reference compounds **6a**,**b** (in CH_3CN, $c = 10^{-3}$ M, 0.1 M TBAP, $v = 250$ mV s^{-1}).[a]

	$E^{red}_{1/2}$ [mV]	$E^{ox}_{1/2}$ [mV][b]	$E^{ox}_{1/2}$ [mV][c]	E_{00} [eV]	ΔG_{ET} [eV]
3e	−970	n.m.[d]	1150[e]	2.30	−0.3
3f	−940	1210[f]	–	2.30	–
4e	−870	750[f]	1150[e]	1.96	0.0
4f	−840	820[f]	–	1.96	–
6a[g]	−1250	1040	1150[e]	2.49	−0.2
6b[h]	−1250	1090	–	2.49	–

[a] Referenced against Fc^+/Fc. [b] BDI or bc-BDP chromophore. [c] Group in the 14- or 8-position. [d] Not measurable. [e] Value of dimethoxybenzene. [f] Irreversible peak (E_p). [g] Redox data taken from reference [30c]. [h] Redox data taken from reference [42].

The validity of this assumption can be directly seen from Table 7 and Table S4 in the Supporting Information. Where-

Table 7. Selected spectroscopic data of **3e**,**f** and **4e**,**f** in various solvents.

	Solvent	λ_{abs} [nm]	$fwhm_{abs}$ [cm^{-1}][a]	λ_{em} [nm]	$fwhm_{em}$ [cm^{-1}][a]	$\Delta\tilde{\nu}_{abs\text{-}em}$ [cm^{-1}][b]	Φ_f	τ_f [ns]	k_r [10^8 s^{-1}]	k_{nr} [10^8 s^{-1}]
3e	hexane	547	907	568	944	500	0.32	4.15	0.8	1.6
	MeCN	538	1071	569	1090	894	0.005	0.02	0.3	588
	MeOH	541	996	571	1159	833	0.001	0.03	0.3	312
3f	hexane	548	914	570	902	654	0.32	3.95	0.8	1.7
	MeCN	538	1029	571	1095	914	0.006	0.15	0.4	66
	MeOH	542	1001	572	1031	834	0.008	0.19	0.4	52
4e	hexane	638	848	655	683	386	0.35	6.53	0.5	1.0
	MeCN	634	867	662	834	592	0.018	0.22	0.8	44
	MeOH	636	871	661	855	517	0.046	0.37[c]	[c]	[c]
4f	hexane	637	702	654	678	382	0.44	6.09	0.7	0.9
	MeCN	633	784	662	857	639	0.43	6.52	0.7	0.9
	MeOH	634	918	664	867	652	0.34	5.84	0.6	1.1

[a] Obtained from the data treatment and fitting procedure described in the text and Supporting Information, fwhm ± 10 cm^{-1}. [b] Obtained as described in the Experimental Section. [c] Biexponential decay with a second $\tau_f = 3.47$ ns, see ref. [52]; k_r and k_{nr} data not determined.

as **4f**, for instance, shows strong emission in solvents of high and low polarity, the fluorescence of **4e** is progressively quenched upon going from hexane to methanol. The quenching characteristics are again similar to those reported for **4b**,**c** above; that is, significant spectral shifts are not noticed and the fluorescence lifetime concomitantly decreases. A plot of the nonradiative rate constant versus the solvent polarity function shows a very similar development (Figure 7). Apparently, the acceptor-modified BDI core is

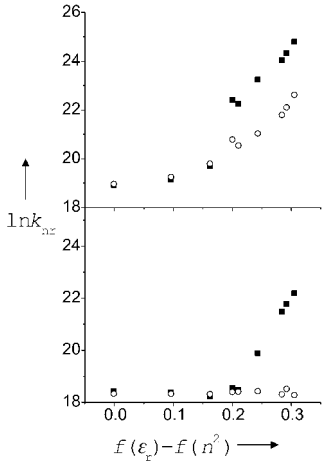

Figure 7. Plot of the nonradiative rate constant vs solvent polarity for **3e** (■) and **3f** (○), both in the upper part, as well as **4e** (■) and **4f** (○) in the lower part (data from Tables S3 and S4 in the Supporting Information; for solvent key, see Figure 4).

now strong enough to activate an electron-transfer process from the considerably weak benzocrown donor. Furthermore, an advantageous side-effect of the substitution of the BDI core is the fact that both the absorption and emission band maxima shift by ≈40 nm to the red and are now found in a wavelength range for which a variety of low-cost laser diodes (e.g., of AlGaInP- or GaInP-type) are commercially available. Spectral analysis by means of the deconvolution and fitting procedure introduced previously reveals very similar behavior as for the nonacceptor-substituted BDIs; that is, narrowing bands and Stokes shifts on decreasing the solvent polarity (Table 7 and Table S4 in the Supporting Information). The ester groups themselves do not seem to have a pronounced influence on the polymethinic conjugation within the chromophore other than introducing a higher degree of flexibility. While the spectra are broadened, as manifested in a fwhm = 784 versus 537 cm^{-1} of the subbands of **4e** versus **4d** in acetonitrile, the molar extinction coefficients are reduced, for example, $\varepsilon_{634} = 68\,600 \pm 400\ M^{-1}\,cm^{-1}$ versus $\varepsilon_{598} = 112\,760\ M^{-1}\,cm^{-1}$ for this pair of dyes, with the integral strength of the transition remaining very similar with $f^{osz}_{S1\leftarrow S0}(\mathbf{4e})/f^{osz}_{S1\leftarrow S0}(\mathbf{4d}) = 1.05$. Moreover, a comparison of the observed and the calculated radiative rate constants performed in the same way as outlined above also yields ratios of $k_r/k_r^{calcd} = 1.00 \pm 0.05$ for **3e** and **4e** in acetonitrile and dibutyl ether; this supports the composite dye model and the polymethinic nature of the ester-substituted chromophore.

Temperature-dependent studies carried out as described above revealed the typical electron-transfer-type quenching features. Upon reducing the temperature, the absorption and emission bands become narrower and more structured, and shift by ≈8 nm to the red in the glass. The fluorescence decays are singly exponential, and the increase in lifetime is pronounced for **4e**, from 1.75 to 7.36 ns, yet less dramatic for **4f**, from 6.12 to 6.33 ns at 299 and 77 K, respectively.

A remarkable effect, however, is found for **3e**,**f**. For these two dyes, not only does **3e** show a reduced fluorescence in polar solvents relative to **3f**, but the fluorescence of the model dye **3f** itself is quenched upon increasing the polarity of its environment, a behavior that is evidently independent of the CT process described so far (Figure 7, Table 7, and Table S3 in the Supporting Information). The effect of ester substitution on the spectral band positions is yet again comparable to their BDI relatives, that is, they are bathochromically shifted by λ ≈ 25 nm (Figure 8). Also in agreement with

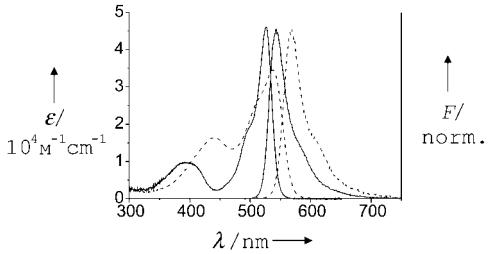

Figure 8. Absorption and fluorescence spectra of **3d** (——) and **3e** (-----) in acetonitrile.

the general optical excitation features of the BDI dyes are the relationships of the integral $S_1 \leftarrow S_0$ transitions and the molar extinction coefficients between **3d** and **3e**, the quotient of the integrals amounting to 0.99 and the respective value of **3e** being $\varepsilon_{538} = 34\,540 \pm 580\ M^{-1}\,cm^{-1}$.[51]

Besides the fact that the two lowest transitions are not well-separated anymore for **3e**,**f** (see, for example, Figure 8), the mirror-image relationship between absorption and fluorescence spectra is fulfilled. Thus, apparently, the accelerated radiationless deactivation of **3f** is not caused by a different emitting species, accelerated internal conversion, or any pronounced conformational changes between the Franck–Condon and the fluorescing excited state, but to the activation of another "dark" deexcitation channel. Keeping in mind that the most stable conformation of **3e** in the crystalline state is a "butterfly"-like kinked geometry (see the section on X-ray diffraction), we tentatively assume that we observed here, for the first time, the solvatokinetically controlled activation of a nonfluorescent competitor state postulated recently by Lindsey et al.[22f] Inspection of the theoretical results in that work suggested that this "butterfly"-type species has a certain charge-transfer character and should possess a higher dipole moment than the planar conformer. Thus, its formation might be facilitated with increasing solvent polarity and might lead to the quenching observed here for **3f**.[53] In the highly rigid and conjugated BDI chromophore, such a bending motion should be much less favored

and interference by this quenching channel is not expected. The data in Table 7 support these considerations.

A study of the effect of temperature variation on the spectroscopic properties of the ester-substituted dyes **3e**,**f** promised a better picture of the quenching process. As would be expected, the spectroscopic changes upon steadily reducing the temperature of solutions of **3f** in ethanol as well as going from 299 K to 77 K for **3e** are small and in agreement with the previous results. Moreover, the increase in fluorescence yield is in accordance with the other low-temperature data as well, resulting in lifetime changes from 0.39 to 5.13 ns and from 0.09 to 5.15 ns at 299 and 77 K for **3f** and **3e**, respectively. An Arrhenius-type analysis of the temperature-dependent fluorescence behavior of **3f** in ethanol (Figure 9) gave an activation barrier of 5.5 kJ mol^{-1} for

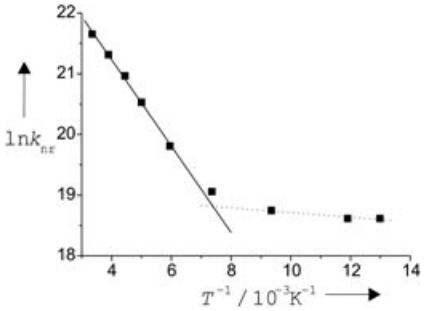

Figure 9. Plot of $\ln k_{nr}$ versus T^{-1} for **3f** in ethanol. The temperature dependence above (——) and below (virtually constant, •••••) the glass temperature of ethanol are indicated.

the quenching reaction. Comparison with literature data on other polyaromatic compounds in which such a structural relaxation pathway in the excited state plays an important role for nonradiative deactivation, for example, 9-*tert*-butyl- or 9-*tert*-pentyl-anthracenes,[54a] suggests that the activation barrier in the present case is rather small. For instance, Jahn and Dreeskamp found an activation energy of 17.5 kJ mol^{-1} for such a process in 9-*tert*-butyl-anthracene in ethanol.[54a] Moreover, as in the case of the anthracenes, a certain "butterfly"-like asymmetry in the ground state of the molecule seems to facilitate the reaction.[54b]

However, recent solvatokinetic studies on the fluorescence behavior of model compound **7b**[22e] show that the intramolecular quenching reactions of the anthracene and the BDP chromophore are not identical. This closely related BDP derivative deviates from **3f** only by the bulkiness of the alkyl substituents in the 1-, 2-, 6-, and 7-positions—the bicyclo skeleton versus methyl and ethyl groups—and also possesses a kinked conformation in the crystalline state (≈ 13.3° as derived from the X-ray structure given in reference [22e]). In contrast to **3f**, however, **7b** exhibits the common BDP features of uniform and considerably high fluorescence yields $\Phi_f = 0.26 \pm 0.03$ in solvents of any polarity.[42] Apparently, in the BDP case, not only a prekinked ground-state conformation seems to be the driving force towards this "dark" channel, but most probably the barrier height between the two excited conformers, and thus the probability of the backreaction seems to be a determining factor here. The latter is expected to be lower in **7b**. At the present stage, we cannot provide a more detailed picture; however, further studies involving a more sophisticated theoretical treatment as well as femtosecond transient absorption spectroscopy and other model compounds are currently being performed to access the underlying mechanism.

With respect to the dye molecule of predominant analytical interest here, namely **4e**, Figure 10 reveals its favorable

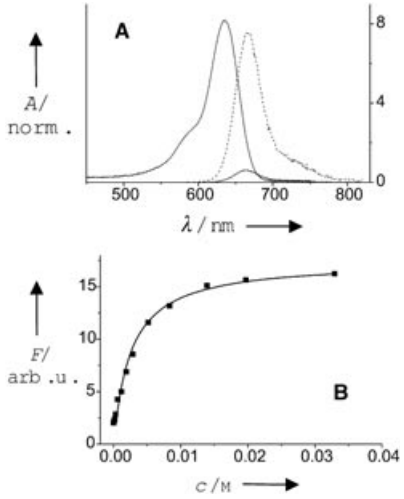

Figure 10. A) Absorption and emission spectra of **4e** (——) and (**4e**)Na^+ (•••••) in methanol. The absorption band of the complex largely overlaps ($\lambda_{max} = 636$ nm) and is omitted for clarity. B) Corresponding, representative titration curve ($c_{\mathbf{4e}} = 2 \times 10^{-6}$ M).

sensing features. Without any pronounced shifts in absorption and emission, the formation of a 1:1 complex of $\log K = 2.35$ stability leads to a ≈8-fold enhanced fluorescence in methanol, Φ_f(**4e**-Na^+) = 0.35, with the typical ET-type characteristics as described above for **4c**.[55] Ca^{2+} and Mg^{2+} do not induce any modulation of the fluorescence, and the effect of K^+ is much less pronounced. In principle, these advantageous features are preserved in water. Unfortunately, the solubility of **4e** in water is not high enough to prevent aggregation. Thus, when attempting a detection of Na^+ with **4e** in highly aqueous media, complicated band shifts are already observed in absorption.[56] We are thus presently following two different routes with this system: modification of the BDI skeleton to improve the actual performance of **4e**, and development of a sensing protocol that can profit from aggregation phenomena.

Conclusion

The present contribution introduced and characterized a new class of strongly absorbing and highly emissive fluorescent dyes that can be used at advantageously long wavelengths. On the basis of preparative pyrrole chemistry, which constitutes an active and intensively studied area of organic chemistry, the facile synthesis in comparatively high yields of a variety of BDI derivatives shown here should stimulate

further research in this area. X-ray structure analyses provided detailed insight into the molecular specifications of these dyes. An important outcome of the work reported here is the interdependence of redox and spectral data. In the same way as the extension of the π system does not dramatically change the energetics that are important for the CT process, it is not expected that a further step to the red by increasing the size and conjugation of the BDI chromophore would have a different impact on such an intramolecular process. However, by simple synthetic means and design considerations it is possible to tune a "silent switch", such as **4d**, to an active one, such as **4e**. Based on this improved understanding of the energetics and photophysics of the bc-BDP and BDI chromophores, we have now a tool in hand that should allow us to custom-design new fluorescent signaling ensembles. Moreover, in addition to supramolecular sensor and switch chemistry as well as electron- or energy-transfer cascades or arrays, such functional dyes are promising candidates for new active materials for dye lasers, organic light-emitting diodes, or other redox-controlled optical applications; they are also expected to give new impulses to labeling chemistry for imaging applications.

Experimental Section

Materials: Metal perchlorates purchased from Aldrich were of highest purity available and were dried in a vacuum oven before use.[57] $HClO_4$, 70% Suprapur from Merck, was used for the protonation experiments. The dyes used for the determination of the relative fluorescence quantum yields and the calibration of the laser impulse fluorometer were obtained from Lambda Physik GmbH (Göttingen, Germany). All the solvents employed were of UV spectroscopic grade (Aldrich, Merck, and Fluka).

General synthesis methods: All syntheses were carried out under a nitrogen atmosphere. Unless otherwise noted, all reagents or solvents were of commercial reagent grade and were used without further purification. Dry dichloromethane and *N*-ethyl-*N*,*N*-diisopropylamine were obtained by refluxing and distilling over CaH_2 under inert atmospheres. Dry THF was distilled from sodium/benzophenone under an inert atmosphere. Column chromatography and TLC were carried out on C-200 (Wakogel) and Kieselgel 60 F254 (Merck), respectively. Melting points were measured with a Yanagimoto BY-1 apparatus. ^{1}H NMR and ^{13}C NMR spectra were recorded in $CDCl_3$ on a JEOL EX 400 spectrometer at ambient temperature. NMR chemical shifts are expressed relative to TMS as the internal standard. IR and UV/Vis spectra were obtained with Hitachi 270–30 and Shimadzu UV-2200 spectrometers, respectively. Mass spectra were measured with a JEOL JMS-700 spectrometer (20 eV for EI and *m*-nitrobenzyl alcohol as matrix for FAB). Elemental analyses were performed with a Yanako MT-5 recorder. DSC and TG experiments were performed on a Seiko Instruments EXSTAR 6000 apparatus.

2-Methyl-4,7-dihydro-4,7-ethano-2*H*-isoindole (2): $LiAlH_4$ (759 mg, 20 mmol) powder was added in small portions over a period of 30 min to a stirred solution of ethyl 4,7-dihydro-4,7-ethano-2*H*-isoindole-1-carboxylate[31] (869 mg, 4 mmol) in dry THF (100 mL) under argon, and the reaction mixture was refluxed for 2 h. After cooling to room temperature, water (50 mL) was added dropwise, and the resulting mixture was filtered through a Celite pad, which was washed with EtOAc (3×50 mL). The organic layer was separated, and the aqueous layer was extracted with EtOAc (2×20 mL). The combined organic layers were washed with water (5×50 mL) and brine (30 mL), dried over Na_2SO_4, and concentrated at reduced pressure. The residue was purified by chromatography on silica gel (50% $CHCl_3$/hexane) to give 573 mg (yield 90%) of **2** as colorless plates. M.p. 129–130 °C; ^{1}H NMR (400 MHz, $CDCl_3$): $\delta = 8.40$ (s, 1H), 7.22 (s, 1H), 6.50–6.45 (m, 2H), 3.76 (m, 2H), 2.19 (s, 3H), 1.57–1.43 ppm (m, 4H); ^{13}C NMR (100 MHz, $CDCl_3$): $\delta = 11.09$, 27.42, 27.50, 32.22, 33.33, 105.57, 117.18, 125.24, 129.47, 136.07, 136.40 ppm; MS (EI): *m*/*z*: 159 $[M]^+$, 131 $[M-C_2H_4]^+$; elemental analysis calcd (%) for $C_{11}H_{13}N$: C 82.97, H 8.23, N 8.80; found: C 82.82, H 8.05, N 8.83.

General procedure for the preparation of 3a–d: Compound **2** (2 mmol) and an aldehyde [benzaldehyde (**3a**), 4-(dimethylamino)benzaldehyde[58] (**3b**), *N*-(4′-formylphenyl)aza[15]crown-5[59] (**3c**) or 15-formylbenzo[15]crown-5 (**3d**); 1 mmol] were dissolved in dry CH_2Cl_2 (100 mL) under nitrogen. One drop of trifluoroacetic acid (TFA) was added, and the solution was stirred at room temperature in the dark for 2–4 h (until TLC indicated complete consumption of the aldehyde). A solution of dichlorodicyanobenzoquinone (DDQ, 1 mmol) in dry CH_2Cl_2 (20 mL) was added, and the mixture was stirred for additional 15 min. The reaction mixture was then treated with *N*-ethyl-*N*,*N*-diisopropylamine (3 mL) and boron trifluoride etherate (3 mL). After stirring for another 30 min, the dark brown solution was washed with water (3×20 mL) and brine (30 mL), dried over Na_2SO_4, and concentrated at reduced pressure. The crude product was purified by silica-gel flash column chromatography and recrystallization from $CHCl_3$/hexane.

*7,7-Difluoro-5,9-dimethyl-14-phenyl-1,4,10,13-tetrahydro-1,4;10,13-bisethano-7-bora-7H-benzo[1,2-a;4,5-a′]diisoindole (**3a**)*: Diisoindole **3a** was prepared from the reaction of **2** (318 mg, 2 mmol) and benzaldehyde (106 mg, 1 mmol) in dry CH_2Cl_2 (100 mL) under nitrogen. The crude product was purified by chromatography (silica gel, 10% EtOAc/hexane). Recrystallization from $CHCl_3$/hexane yielded orange-red, metallike shining crystals (190 mg, yield 42%). M.p. 196 °C (decomp); ^{1}H NMR (400 MHz, $CDCl_3$): $\delta = 7.57$–7.39 (m, 5H), 6.40–6.36 (m, 2H), 6.08–6.03 (m, 2H), 3.80–3.82 (m, 2H), 2.61 (m, 2H), 2.53 (s, 6H), 1.15–1.42 ppm (m, 8H); ^{13}C NMR (100 MHz, $CDCl_3$): $\delta = 12.52$ (both), 25.84 (one diastereomer), 25.88 (other diastereomer), 26.42 (one diastereomer), 26.48 (other diastereomer), 32.87 (both), 35.16 (both), 110.40 (both), 121.74 (one diastereomer), 121.77 (other diastereomer), 127.75 (both), 130.5 (both), 130.90 (both), 134.20 (one diastereomer), 134.29 (other diastereomer), 135.82 (one diastereomer), 135.84 (other diastereomer), 140.62 (one diastereomer), 140.65 (other diastereomer), 146.41 (both), 148.57 (both), 150.11 ppm (both); IR (KBr): $\tilde{\nu} = 1562$, 1509 (C=C, C=N), 1197 cm^{-1} (B–F); MS (EI): *m*/*z*: 452 $[M]^+$, 396 $[M-2C_2H_4]^+$; elemental analysis calcd (%) for $C_{29}H_{27}BF_2N_2 \cdot {}^1/_2H_2O$: C 75.50, H 6.12, N 6.07; found: C 75.23, H 6.05, N 6.03.

*7,7-Difluoro-5,9-dimethyl-14-[4-(dimethylamino)phenyl]-1,4,10,13-tetrahydro-1,4;10,13-bisethano-7-bora-7H-benzo[1,2-a;4,5-a′]diisoindole (**3b**)*: Acid-catalyzed condensation of **2** (318 mg, 2 mmol) and 4-(dimethylamino) benzaldehyde (149 mg, 1 mmol) in dry CH_2Cl_2 (100 mL) at room temperature, followed by flash chromatography (silica gel, 10% EtOAc/hexane) and recrystallization from $CHCl_3$/hexane yielded red crystals (258 mg, yield 52%). M.p. 200 °C (decomp); ^{1}H NMR (400 MHz, $CDCl_3$): $\delta = 7.23$–7.25 (m, 2H), 6.79–6.81 (m, 2H), 6.38–6.41 (m, 2H), 6.1–6.15 (m, 2H), 3.8–3.81 (m, 2H), 3.10 (s, 6H), 2.93–3.07 (m, 2H), 2.52 (s, 6H), 1.18–1.44 ppm (m, 8H); ^{13}C NMR (100 MHz, $CDCl_3$): $\delta = 12.48$ (both), 25.94 (one diastereomer), 25.98 (other diastereomer), 26.52 (one diastereomer), 26.60 (other diastereomer), 32.89 (both), 35.28 (one diastereomer), 35.31 (other diastereomer), 40.37 (both), 111.09 (both), 122.19 (one diastereomer), 122.21 (other diastereomer), 127.81 (both), 129.92 (one diastereomer), 130.25 (other diastereomer), 130.65 (both), 134.20 (one diastereomer), 134.28 (other diastereomer), 135.87 (both), 137.67 (both), 140.63 (one diastereomer), 140.65 (other diastereomer), 146.55 (both), 150.16 (one diastereomer), 150.87 ppm (other diastereomer); IR (neat): $\tilde{\nu} = 1566$, 1504 (C=C, C=N), 1188 cm^{-1} (B–F); MS (EI): *m*/*z*: 495 $[M]^+$, 439 $[M-2C_2H_4]^+$; elemental analysis calcd (%) for $C_{31}H_{32}BF_2N_3$: C 75.16, H 6.51, N 8.48; found: C 75.12, H 6.50, N 8.45.

*7,7-Difluoro-5,9-dimethyl-14-[4-(1,4,7,10,13-azatetraoxaheptadecanyl)-phenyl]-1,4,10,13-tetrahydro-1,4;10,13-bisethano-7-bora-7H-benzo[1,2-a;4,5-a′]diisoindole (**3c**)*: Diisoindole **3c** was prepared from acid-catalyzed condensation of **2** (318 mg, 2 mmol) and *N*-(4′-formylphenyl)-aza[15]crown-5 (323 mg, 1 mmol) in dry CH_2Cl_2 (100 mL) and purified by flash chromatography (silica gel, 50% EtOAc/$CHCl_3$) followed by recrystallization from $CHCl_3$/hexane to yield orange-red crystals (482 mg, yield 72%). M.p. 192 °C (decomp); ^{1}H NMR (400 MHz, $CDCl_3$): $\delta = 7.20$–7.22 (m, 2H), 6.73–6.75 (m, 2H), 6.38–6.4 (m, 2H), 6.14–6.15 (m, 2H), 3.85–3.87 (m, 2H), 3.82 (m, 2H), 3.67–3.71 (m, 18H), 3.0 (m, 2H), 2.51 (s, 6H), 1.21–1.45 ppm (m, 8H); ^{13}C NMR (100 MHz, $CDCl_3$): $\delta = 12.45$ (both), 25.93 (one diastereomer), 25.98 (other diastereomer), 26.51 (one

diastereomer), 26.60 (other diastereomer), 32.88 (both), 35.31 (one diastereomer), 35.34 (other diastereomer), 52.79 (both), 68.55 (both) , 69.84 (both), 70.26 (both), 71.27 (both), 110.40 (both) , 121.74 (one diastereomer), 121.77 (other diastereomer), 127.75 (both), 130.17 (one diastereomer), 130.5 (other diastereomer), 130.90 (both), 134.20 (one diastereomer), 134.29 (other diastereomer), 135.82 (one diastereomer), 135.84 (other diastereomer), 140.62 (one diastereomer), 140.65 (other diastereomer), 146.41 (both), 148.57 (both), 150.11 ppm (both); IR (neat): $\tilde{\nu}$ = 1558, 1508 (C=C, C=N), 1195 cm^{-1} (B–F); MS (FAB): *m/z*: 670 $[M+H]^+$; elemental analysis calcd (%) for $C_{39}H_{46}BF_2N_3O_4 \cdot {}^1/_2H_2O$: C 69.02, H 6.98, N 6.19; found: C 68.92, H 6.83, N 6.11.

*7,7-Difluoro-5,9-dimethyl-14-(1,4,7,10,13-pentaoxabenzoheptadecan-15-yl)-1,4,10,13-tetrahydro-1,4;10,13-bisethano-7-bora-7H-benzo[1,2-a;4,5-a′]diisoindole (**3d**)*: Diisoindole **3d** was prepared from the acid-catalyzed condensation of **2** (318 mg, 2 mmol) and 15-formylbenzo[15]crown-5 (296 mg, 1 mmol) in dry CH_2Cl_2 (100 mL), and purified by flash chromatography (silica gel, 50% EtOAc/$CHCl_3$) followed by recrystallization from $CHCl_3$/hexane to yield orange-red crystals (372 mg, yield 58%). M.p. 192°C (decomp); ^{1}H NMR (400 MHz, $CDCl_3$): δ = 6.93–6.99 (m, 3H), 6.38–6.41 (m, 2H), 6.09–6.11 (m, 2H), 4.27 (m, 2H), 4.1 (m, 2H), 4.01–4.02 (m, 2H), 3.92–3.94 (m, 2H), 3.81–3.83 (m, 10H), 2.82 (m, 2H), 2.52 (s, 6H), 1.15–1.44 ppm (m, 8H); ^{13}C NMR (100 MHz, $CDCl_3$): δ = 12.52 (both), 25.88 (one diastereomer), 25.92 (other diastereomer), 26.51 (one diastereomer), 26.57 (other diastereomer), 32.90 (one diastereomer), 32.92 (other diastereomer), 35.26 (one diastereomer), 35.28 (other diastereomer), 68.39 (both), 68.72 (both), 69.21 (both), 69.23 (both), 69.36 (both), 70.14 (both), 70.98 (both), 71.06 (both), 112.3 (both), 114.3 (one diastereomer), 114.4 (other diastereomer), 122.0 (one diastereomer), 122.44 (other diastereomer), 127.33 (one diastereomer), 127.38 (other diastereomer), 127.41 (one diastereomer), 127.5 (other diastereomer), 134 (both), 135.84 (both), 135.90 (one diastereomer), 135.93 (other diastereomer), 138.0 (one diastereomer), 138.82 (other diastereomer), 147.4 (both), 148.35 (one diastereomer), 148.4 (other diastereomer), 149.6 (both), 150.2 ppm (both); IR (neat): $\tilde{\nu}$ = 1562, 1504 (C=C, C=N), 1187 cm^{-1} (B–F); MS (EI): *m/z*: 642 $[M]^+$, 623 $[M-F]^+$, 586 $[M-2C_2H_4]^+$; elemental analysis calcd (%) for $C_{37}H_{41}BF_2N_2O_5 \cdot {}^1/_3H_2O$: C 68.52, H 6.48, N 4.32; found: C 68.54, H 6.43, N 4.33.

General procedure for the preparation of 3e and 3f: Compound **1** (2 mmol) and 15-formylbenzo[15]crown-5 (**3e**, 1 mmol) or benzaldehyde (**3f**, 1 mmol) were dissolved in dry CH_2Cl_2 (100 mL) under nitrogen. One drop of TFA was added, and the solution was refluxed in the dark for 12 h (until TLC indicated complete consumption of the aldehyde). After cooling to room temperature, a solution of DDQ (1 mmol) in dry CH_2Cl_2 (20 mL) was added, and the mixture was stirred for additional 15 min. The reaction mixture was then treated with *N*-ethyl-*N*,*N*-diisopropylamine (3 mL) and boron trifluoride etherate (3 mL). After stirring for another 30 min, the dark brown solution obtained was washed with water (3×20 mL) and brine (30 mL), dried over Na_2SO_4, and concentrated under reduced pressure. The crude product was purified by silica gel flash column chromatography and recrystallization from $CHCl_3$/hexane.

*Diethyl-7,7-difluoro-14-(1,4,7,10,13-pentaoxabenzoheptadecan-15-yl)-1,4,10,13-tetrahydro-1,4;10,13-bisethano-7-bora-7H-benzo[1,2-a;4,5-a′]diisoindole-5,9-dicarboxylate (**3e**)*: Dicarboxylate **3e** was prepared from the acid-catalyzed condensation of **1** (434 mg, 2 mmol) and 15-formylbenzo[15]crown-5 (296 mg, 1 mmol) in dry dichloromethane (100 mL), and was purified by chromatography (silica gel, 50% EtOAc/$CHCl_3$) and recrystallization from $CHCl_3$/hexane to yield red crystals (258 mg, yield 34%). M.p. 140°C (decomp); ^{1}H NMR (400 MHz, $CDCl_3$): δ = 6.92–7.05 (m, 3H), 6.39–6.44 (m, 2H), 6.09–6.11 (m, 2H), 4.45 (q, *J* = 7.3 Hz, 4H), 4.30 (m, 4H), 4.10–4.12 (m, 2H), 4.02–4.04 (m, 2H), 3.94–3.96 (m, 2H), 3.81–3.83 (m, 8H), 2.81 (m, 2H), 1.45 (t, *J* = 7.3 Hz, 6H), 1.14–1.29 ppm (m, 8H); ^{13}C NMR (100 MHz, $CDCl_3$): δ = 14.10 (both), 25.67 (one diastereomer), 25.87 (other diastereomer), 26.11 (both), 34.09 (both), 35.51 (both), 61.56 (both), 65.82 (both), 68.32 (both), 68.84 (both), 69.07 (both), 69.18 (both), 70.02 (both), 70.08 (both), 70.9 (both), 70.96 (both), 112.25 (both), 113.9 (one diastereomer), 114.16 (other diastereomer), 121.84 (one diastereomer), 122.33 (other diastereomer), 126.43 (both), 130.46 (both), 133.60 (both), 135.92 (one diastereomer), 135.98 (other diastereomer), 138.26 (both), 142.44 (both), 147.72 (one diastereomer), 148.72 (other diastereomer), 150.58 (both), 153.17 (both), 161.02 ppm (both); IR (neat): $\tilde{\nu}$ = 1546, 1512 (C=C, C=N), 1192 cm^{-1} (B–F); MS (FAB): *m/z*: 759 $[M+H]^+$; elemental analysis calcd (%) for $C_{41}H_{45}BF_2N_2O_9$: C 64.91, H 5.98, N 3.69; found: C 64.62, H 6.01, N 3.65.

*Diethyl-7,7-difluoro-14-phenyl-1,4,10,13-tetrahydro-1,4;10,13-bisethano-7-bora-7H-benzo[1,2-a;4,5-a′]diisoindole-5,9-dicarboxylate (**3f**)*: Dicarboxylate **3f** was prepared from the acid-catalyzed condensation of **1** (434 mg, 2 mmol) and benzaldehyde (106 mg, 1 mmol) in dry CH_2Cl_2 (100 mL) under nitrogen. It was purified by chromatography (silica gel, 50% EtOAc/$CHCl_3$) and recrystallization from $CHCl_3$/hexane to yield red crystals (210 mg, yield 37%). M.p. 130°C (decomp); ^{1}H NMR (400 MHz, $CDCl_3$): δ = 7.57–7.68 (m, 3H), 7.40–7.42 (m, 2H), 6.38–6.42 (m, 2H), 6.03–6.06 (m, 2H), 4.46 (q, *J* = 7.3 Hz, 4H), 4.31 (m, 2H), 2.57–2.59 (m, 2H), 1.46 (t, *J* = 7.3 Hz, 6H), 1.13–1.42 ppm (m, 8H); ^{13}C NMR (100 MHz, $CDCl_3$): δ = 14.12 (both), 25.57 (one diastereomer), 25.85 (other diastereomer), 26.12 (both), 34.09 (both), 35.53 (both), 61.55 (both), 65.83 (both), 110.37 (both), 121.69 (one diastereomer), 121.73 (other diastereomer), 127.73 (both), 130.3 (both), 130.92 (both), 134.19 (one diastereomer), 134.27 (other diastereomer), 135.77 (one diastereomer), 135.81 (other diastereomer), 140.61 (one diastereomer), 140.63 (other diastereomer), 146.39 (both), 148.53 (both), 150.13 ppm (both); IR (neat): $\tilde{\nu}$ = 1558, 1510 (C=C, C=N), 1190 cm^{-1} (B–F); MS (EI): *m/z*: 568 $[M]^+$, 540 $[M-C_2H_4]^+$; elemental analysis calcd (%) for $C_{33}H_{31}BF_2N_2O_4 \cdot {}^1/_2H_2O$: C 68.64, H 5.58, N 4.85; found: C 68.77, H 5.46, N 4.83.

General procedure for the preparation of 4a–f: Compounds **3a–f** were heated at 220°C under N_2 at reduced pressure (10 mmHg) to afford quantitative yields of the corresponding pure **4a–f**.

*7,7-Difluoro-5,9-dimethyl-14-phenyl-7-bora-7H-benzo[1,2-a;4,5-a′]diisoindole (**4a**)*: Copper-colored crystals; m.p. >250°C; ^{1}H NMR (400 MHz, $CDCl_3$): δ = 7.64–7.68 (m, 5H), 7.51–7.53 (m, 2H), 7.08–7.11 (m, 2H), 6.98–7.02 (m, 2H), 6.16–6.18 (m, 2H), 2.97 ppm (s, 6H); ^{13}C NMR (100 MHz, $CDCl_3$): δ = 12.45, 121.18, 121.94, 123.75, 124.76, 128.72, 129.01, 129.20, 129.38, 130.50, 130.53, 133.89, 135.05, 150.41 ppm; IR (neat): $\tilde{\nu}$ = 1542, 1510 (C=C, C=N), 1191 cm^{-1} (B–F); MS (EI): *m/z*: 396 $[M]^+$; elemental analysis calcd (%) for $C_{25}H_{19}BF_2N_2 \cdot H_2O$: C 72.49, H 5.11, N 6.76; found: C 72.73, H 4.82, N 6.77.

*7,7-Difluoro-5,9-dimethyl-14-[4-(dimethylamino)phenyl]-7-bora-7H-benzo[1,2-a;4,5-a′]diisoindole (**4b**)*: Copper-colored crystals; m.p. >250°C; ^{1}H NMR (400 MHz, $CDCl_3$) δ = 7.63–7.65 (m, 2H), 7.30–7.32 (m, 2H), 7.01–7.11 (m, 4H), 6.91–6.93 (m, 2H), 6.43–6.45(m, 2H), 3.13 (s, 6H), 2.95 ppm (s, 6H); ^{13}C NMR (100 MHz, $CDCl_3$): δ = 12.41, 40.44, 112.55, 121.61, 121.74, 122.19, 123.55, 125.51, 128.54, 129.75, 130.38, 134.06, 135.96, 149.68, 150.85 ppm; IR (neat): $\tilde{\nu}$ = 1531, 1508 (C=C, C=N), 1195 cm^{-1} (B–F); MS (EI): *m/z*: 439 $[M]^+$; elemental analysis calcd (%) for $C_{27}H_{24}BF_2N_3$: C 73.82, H 5.51, N 9.56; found: C 73.77, H 5.58, N 9.44.

*7,7-Difluoro-5,9-dimethyl-14-[4-(1,4,7,10,13-azatetraoxaheptadecanyl)-phenyl]-7-bora-7H-benzo[1,2-a;4,5-a′]diisoindole (**4c**)*: Copper-colored crystals; m.p. >250°C; ^{1}H NMR (400 MHz, $CDCl_3$): δ = 7.63–7.65 (m, 2H), 7.27–7.29 (m, 2H), 7.07–7.11 (m, 4H), 6.86–6.88 (m, 2H), 6.48–6.50 (m, 2H), 3.89–3.91 (m, 2H), 3.63–3.74 (m, 18H), 2.96 ppm (s, 6H); ^{13}C NMR (100 MHz, $CDCl_3$): δ = 14.12, 52.81, 68.57, 69.86, 70.27, 71.33, 112.40, 121.67, 121.75, 127.95, 130.67, 131.43, 134.07, 135.37, 136.63, 141.67, 146.61, 149.57, 150.91 ppm; IR (neat): $\tilde{\nu}$ = 1538, 1508 (C=C, C=N), 1195 cm^{-1} (B–F); MS (EI): *m/z*: 613 $[M]^+$; elemental analysis calcd (%) for $C_{35}H_{38}BF_2N_3O_4$: C 68.52, H 6.24, N 6.85; found: C 68.45, H 6.32, N 6.78.

*7,7-Difluoro-5,9-dimethyl-14-(1,4,7,10,13-pentaoxabenzoheptadecan-15-yl)-7-bora-7H-benzo[1,2-a;4,5-a′]diisoindole (**4d**)*: Copper-colored crystals; m.p. >250°C; ^{1}H NMR (400 MHz, $CDCl_3$): δ = 7.64–7.66 (m, 2H), 7.0–7.13 (m, 7H), 6.34–6.36 (m, 2H), 4.31–4.33 (m, 2H), 4.05–4.09 (m, 4H), 3.81–3.87 (m, 10H), 2.95 ppm (s, 6H); ^{13}C NMR (100 MHz, $CDCl_3$): δ = 12.43, 68.48, 68.50, 69.16, 69.41, 70.16, 70.17, 71.00, 71.11, 113.66, 113.81, 121.50, 121.65, 121.85, 123.80, 125.00, 127.52, 128.92, 130.42, 133.84, 134.48, 149.55, 149.60, 150.28 ppm; IR (neat): $\tilde{\nu}$ = 1538, 1509 (C=C, C=N), 1192 cm^{-1} (B–F); MS (EI): *m/z*: 586 $[M]^+$; elemental analysis calcd (%) for $C_{33}H_{33}BF_2N_2O_5 \cdot H_2O$: C 65.57, H 5.84, N 4.63; found: C 65.55, H 5.74, N 4.37.

*Diethyl-7,7-difluoro-14-(1,4,7,10,13-pentaoxabenzoheptadecan-15-yl)-7-bora-7H-benzo[1,2-a;4,5-a′]diisoindole-5,9-dicarboxylate (**4e**)*: Blue powder; m.p. 143–145°C; ^{1}H NMR (400 MHz, $CDCl_3$): δ = 8.10–8.12 (m, 2H), 7.26–7.30 (m, 4H), 6.99–7.19 (m, 3H), 6.36–6.38 (m, 2H), 4.61 (q,

$J=7.3$ Hz, 4H), 4.33 (m, 2H), 4.05–4.08 (m, 4H), 3.81–3.86 (m, 10H), 1.55 ppm (t, $J=7.3$ Hz, 6H); ^{13}C NMR (100 MHz, $CDCl_3$): $\delta=14.14$, 62.21, 62.30, 68.36, 68.52, 68.99, 69.22, 70.04, 70.04, 70.90, 71.00, 113.06, 121.24, 122.07, 124.04, 126.51, 126.57, 129.42, 129.92, 131.14, 134.64, 140.03, 141.06, 149.88, 150.17, 160.63 ppm; IR (neat): $\tilde{\nu}=1546$, 1511 (C=C, C=N), 1192 cm^{-1} (B–F); MS (FAB): m/z: 703 $[M+H]^+$; elemental analysis calcd (%) for $C_{37}H_{37}BF_2N_2O_9$: C 63.26, H 5.31, N 3.99; found: C 62.98, H 5.09, N 3.90.

*Diethyl-7,7-difluoro-14-phenyl-7-bora-7H-benzo[1,2-a;4,5-a′]diisoindole-5,9-dicarboxylate (**4f**)*: Copper-colored crystals; m.p. >250 °C; ^{1}H NMR (400 MHz, $CDCl_3$): $\delta=8.18$–8.20 (m, 2H), 7.52–7.71 (m, 5H), 7.21–7.25 (m, 2H), 6.95–6.99 (m, 2H), 6.11–6.13 (m, 2H), 4.58 (q, $J=7.3$ Hz, 4H), 1.56 ppm (t, $J=7.3$ Hz, 6H); ^{13}C NMR (100 MHz, $CDCl_3$): $\delta=14.14$, 62.21, 68.36, 121.17, 121.97, 123.75, 124.77, 128.75, 129.02, 129.23, 129.43, 130.51, 130.57, 133.92, 135.15, 150.50 ppm; IR (neat): $\tilde{\nu}=1546$, 1509 (C=C, C=N), 1191 cm^{-1} (B–F); MS (EI): m/z: 512 $[M]^+$, 464 $[M-BF_2]^+$; elemental analysis calcd (%) for $C_{29}H_{23}BF_2N_2O_4$: C 67.99, H 4.53, N 5.47; found: C 67.76, H 4.62, N 5.51.

X-ray crystallography: A summary of the crystallographic data and details of the structure determinations is given in Table 1. The data were collected on a Bruker SMART CCD diffractometer (**3a**,**d** and **4a**,**d**; $Mo_{K\alpha}$ radiation, $\lambda=0.71073$ Å, ω scans), a Rigaku AFC5R diffractometer (**3c**; $Mo_{K\alpha}$ radiation, $2\Theta-\omega$ scans), and a Rigaku/MSC Mercury CCD diffractometer (**3e**; $Mo_{K\alpha}$ radiation, ω scans). The data were corrected for Lorentz and polarization effects, absorption, and secondary extinction. The structures were solved by direct methods and refined by full-matrix least-squares methods based on F^2 (SHELX97[60] for **3a**,**d** and **4a**,**d**, teXsan[61] for **3c**,**e**). In **4a** and **3d**, hydrogen atoms were located by difference Fourier syntheses. For all other compounds, hydrogen positions were calculated in correspondence to their geometrical conditions. It should be noted that **4a** contains a mirror plane which coincides with that of the space group *Pnnm*. For **3a**, the *Pnnm* symmetry is fulfilled only statistically. This leads to an overlap of the double bonds C11=C12 and C15=C16 with the single bonds C11A–C12A and C15A–C16A, respectively. Therefore, four corresponding restraints for bond lengths were used in the structure refinement. In the structure of **3e**, a conformational disorder of the benzocrown ring was observed. This disorder leads to a splitting of one oxygen and three carbon atoms.

CCDC-215231 (**3a**), CCDC-210669 (**3c**), CCDC-214765 (**3d**), CCDC-210668 (**3e**), CCDC-212601 (**4a**), and CCDC-212600 (**4d**) contain the supplementary crystallographic data for this paper. These data can be obtained free of charge via www.ccdc.cam.ac.uk/conts/retrieving.html (or from the Cambridge Crystallographic Data Centre, 12 Union Road, Cambridge CB2 1EZ, UK; fax: (+44) 1223-336033; or deposit@ccdc.cam.uk)

Steady-state absorption and fluorescence spectroscopy: UV/Vis spectra were recorded on a Bruins Instruments Omega 10 spectrophotometer and for the steady-state fluorescence spectra, a Spectronics Instruments 8100 spectrofluorometer was employed. Titrations and low-temperature phosphorescence checks were performed on a Perkin–Elmer LS50B spectrofluorometer. All measurements were carried out at 298±1 K. Molar extinction coefficients were determined from $N=8$ individual samples. For the fluorescence experiments, only dilute solutions with an optical density (OD) below 0.1 at the absorption maximum were used and the fluorescence measurements were performed with a 90° standard geometry and polarizers set at 54.7° (emission) and 0° (excitation). The fluorescence quantum yields (Φ_f) were determined relative to fluorescein 27 in 0.1 N NaOH ($\Phi_f=0.90\pm0.03$)[62] and 4-dicyanomethylene-2-methyl-6-(*p*-dimethylaminostyryl)-4H-pyran in methanol ($\Phi_f=0.43\pm0.08$)[63] for the **3** series as well as rhodamine 101 in ethanol ($\Phi_f=1.00\pm0.02$)[64] for all the compounds of the **4** series, except **4e**,**f**. For the latter, cryptocyanine in ethanol ($\Phi_f=0.007\pm0.001$)[65] was used, which was additionally checked against rhodamine 101 for comparability. All the fluorescence spectra presented here were corrected for the spectral response of the detection system (calibrated quartz halogen lamp placed inside an integrating sphere; Gigahertz-Optik) and for the spectral irradiance of the excitation channel (calibrated silicon diode mounted at a sphere port; Gigahertz-Optik). The uncertainties of the fluorescence quantum yields were determined to ±5% (for $\Phi_f>0.2$), ±10% (for $0.2>\Phi_f>0.02$), ±20% (for $0.02>\Phi_f>5\times10^{-3}$), and ±30% (for $5\times10^{-3}>\Phi_f$). The Stokes shifts were calculated from the differences between the maxima of the lowest/highest energy subband of the corresponding deconvoluted absorption and emission spectra (cf. Figure S4 in the Supporting Information), and not from the global band maxima (in nm) as given in the tables. It should further be noted that in addition to deconvolution, conversion of the fluorescence spectra to the energy scale requires another correction step.[66]

Time-resolved fluorescence spectroscopy: Fluorescence lifetimes (τ_f) were measured with a unique customized laser impulse fluorometer with picosecond time resolution. To be able to excite the BDI dyes in their longest-wavelength absorption band, the setup described by us in an earlier publication[67] was modified with respect to the excitation source. The 80 fs pulses provided at 800 nm with a repetition rate of 82 MHz by a frequency-doubled Nd:YVO_4 laser (Spectra Physics Millennia Xs) pumped Ti:sapphire laser (Spectra Physics Tsunami) were used to seed a regenerative amplifier (Spectra Physics Spitfire P-5K), whereby pulse amplification was obtained by pumping with a frequency-doubled Nd:YLF laser (Spectra Physics Evolution X) operated at 5 kHz. The typically 90 fs long output pulses were fed into an OPA (Spectra Physics OPA-800-F-HGII) and used to generate the respective excitation light by frequency quadrupling the idler of the OPA. The fluorescence was collected at right angles (polarizer set at 54.7°; monochromator with spectral bandwidths of 4, 8, and 16 nm) and the fluorescence decays were recorded with a modular single-photon timing unit described in reference [67]. With typical instrumental response functions of 25–30 ps (full width at half maximum), the time division was 5.2 ps per channel and the experimental accuracy was ±3 ps. The laser beam was attenuated with a double prism attenuator from LTB and typical excitation energies were in the nanowatt-to-microwatt range (average laser power). Other details on the characterization and calibration of the instrument can be found in references [57,67]. The fluorescence lifetime profiles were analyzed with a PC and the software package Global Unlimited V2.2 (Laboratory for Fluorescence Dynamics, University of Illinois). The goodness-of-fit of the single decays, as judged by reduced chi-squared (χ^2_R) and the autocorrelation function $C(j)$ of the residuals, was always below $\chi^2_R<1.2$. For all dyes showing a single fluorescence band, decays were recorded at three different emission wavelengths and analyzed globally. For the dual emissive dyes, decays were recorded at ten different wavelengths over the entire emission spectrum and also analyzed by global analysis. Such a global analysis of decays recorded at different emission wavelengths implies that the decay times of the species are linked while the program varies the preexponential factors and lifetimes until the changes in the error surface (χ^2 surface) are minimal, that is, convergence is reached. The fitting results are judged for every single decay (local χ^2_R) and for all the decays (global χ^2_R). The errors for all the global analytical results presented here were below a global $\chi^2_R=1.2$.

Low-temperature and temperature-dependent measurements: Absorption and fluorescence measurements as a function of temperature or at 77 K were conducted with a continuous flow cryostat CF1204 (Oxford Instruments), modified for us with liquid nitrogen. Liquid N_2 was pumped from a storage container through a transfer tube (GFS300, Oxford Instruments) and flow control (VC30, Oxford Instruments) by a gas flow pump (GF2, Oxford Instruments) through the cryostat. The temperature was externally controlled by heating and flow adjustment with the temperature controller ITC4 (Oxford Instruments). The temperature in the sample rod was monitored by means of the temperature-dependent resistance of a sensor, which was calibrated with a Peltier element. In the cooling regime, the temperature was gradually decreased in steps of 30 K with equilibration times of 20 min at every point of measurement.

Cyclic voltammetry: Cyclic voltammograms were obtained in acetonitrile/0.1 M TBAP (tetra-*n*-butylammonium perchlorate) on a BAS electrochemical analyzer model BS-1 with a platinum disk as the working electrode, $Ag/AgNO_3$ as the quasi-reference electrode, and a platinum wire as the counterelectrode. Redox potentials were referenced internally against ferrocenium/ferrocene (Fc^+/Fc). Measurements were performed under an inert atmosphere with a scan rate of 250 mVs^{-1} at room temperature.

Complex stability constants: The complex stability constants reported here were determined from fluorescence measurements. The complex stability constants K were measured by titrating a dilute solution (typically 10^{-6} M) of ligand by adding aliquots of metal ion solution (c_{M0} titration). Methods detailed in reference [57] based on models introduced by Valeur et al.[68] were employed to fit the complexometric titration data

(with Origin V7.0, Originlab Corp.). The reported values are mean values of at least two measurements with correlation coefficients >0.99.

Quantum chemical calculations: Geometry optimizations were performed employing the semiempirical AM1 method (gradient <0.01) and transition energies were calculated on the basis of these ground state geometries and 1SCF calculations with a CI of 8 by the AM1 method (Ampac V6.55, Semichem).[69]

Acknowledgement

We appreciate financial support from the Grants-in-aid for Scientific Research from the Ministry of Education, Culture, Sports, Science and Technology of Japan. Z.S. is grateful for a JSPS postdoctoral fellowship.

[1] a) R. B. Thompson in *Probe Design and Chemical Sensing* (Ed.: J. R. Lakowicz), Plenum, New York, **1994**, pp. 151–181; b) G. A. Casay, D. B. Shealy, G. Patonay in *Probe Design and Chemical Sensing* (Ed.: J. R. Lakowicz), Plenum, New York, **1994**, pp. 183–222; c) R. P. Haugland, *Handbook of Fluorescent Probes and Research Products*, 9th ed., Molecular Probes, Eugene, OR, **2002**; d) E. U. Akkaya in *Chemosensors of Ion and Molecule Recognition* (Eds.: J.-P. Desvergne, A. W. Czarnik), Kluwer Academic, Dordrecht, **1997**, pp. 177–188; e) E. Terpetschnig, O. S. Wolfbeis in *Near-Infrared Dyes for High Technology Applications* (Eds.: S. Dähne, U. Resch-Genger, O. S. Wolfbeis), Kluwer Academic, Dordrecht, **1998**, pp. 161–182.

[2] R. DeBiasio, G. R. Bright, L. A. Ernst, A. S. Waggoner, D. L. Taylor, *J. Cell Biol.* **1987**, *105*, 1613–1622; G. Patonay, M. D. Antoine, *Anal. Chem.* **1991**, *63*, 321A–327A; A. Becker, C. Hessenius, K. Licha, B. Ebert, U. Sukowski, W. Semmler, B. Wiedenmann, C. Grötzinger, *Nat. Biotechnol.* **2001**, *19*, 327–331; R. Weissleder, U. Mahmood, *Radiology* **2001**, *219*, 316–333; T. F. Massoud, S. S. Gambhir, *Genes Dev.* **2003**, *17*, 545–580.

[3] J. Griffiths, *Chimia* **1991**, *45*, 304–307.

[4] R. A. Wagner, J. S. Lindsey, *J. Am. Chem. Soc.* **1994**, *116*, 9759–9760; A. Harriman, R. Ziessel, *Chem. Commun.* **1996**, 1707–1716; D. J. Cárdenas, J.-P. Collin, P. Gaviña, J.-P. Sauvage, A. De Cian, J. Fischer, N. Armaroli, L. Flamigni, V. Vicinelli, V. Balzani, *J. Am. Chem. Soc.* **1999**, *121*, 5481–5488; A. D. Shukla, B. Ganguly, P. C. Dave, A. Samanta, A. Das, *Chem. Commun.* **2002**, 2648–2649; T. Akasaka, J. Otsuki, K. Araki, *Chem. Eur. J.* **2002**, *8*, 130–136; H. Li, J. O. Jeppesen, E. Levillain, J. Becher, *Chem. Commun.* **2003**, 846–847.

[5] *Dye lasers* (Eds.: F. P. Schäfer, K. H. Drexhage), Springer, Berlin, 3rd ed., **1990**; M. Maeda, *Laser dyes*, Academic Press, Tokyo, **1984**; U. Brackmann, *Lambdachrome Laser Dyes*, 2nd ed., Lambda Physik GmbH, Göttingen, **1994**.

[6] D. J. Williams, *Angew. Chem.* **1984**, *96*, 637–651; *Angew. Chem. Int. Ed. Engl.* **1984**, *23*, 690–703; M. Okawara, T. Kitao, T. Hirashima, M. Matsuoka, *Organic Colorants*, Kodansha, Elsevier, Tokyo, Amsterdam, **1988**; G. M. Tsivgoulis, J.-M. Lehn, *Angew. Chem.* **1995**, *107*, 1188–1191; *Angew. Chem. Int. Ed. Engl.* **1995**, *34*, 1119–1122; M. Matsuoka in *Near-Infrared Dyes for High Technology Applications* (Eds.: S. Dähne, U. Resch-Genger, O. S. Wolfbeis), Kluwer Academic, Dordrecht, **1998**, pp. 203–231; D. S. Tyson, C. A. Bignozzi, F. N. Castellano, *J. Am. Chem. Soc.* **2002**, *124*, 4562–4563.

[7] G. Bach, S. Dähne in *Rodd's Chemistry of Carbon Compounds*, *Vol. IVB* (Ed.: M. Sainsbury), Elsevier, Amsterdam, 2nd ed., **1997**, pp. 383–481.

[8] a) S. Dähne, *Science* **1978**, *199*, 1163–1167; b) S. Dähne, F. Moldenhauer, *Prog. Phys. Org. Chem.* **1985**, *15*, 1–130.

[9] S. Dähne, D. Leupold, *Ber. Bunsen-Ges.* **1966**, *70*, 618–625.

[10] A. D. Kachkovskii, *Russ. Chem. Rev.* **1997**, *66*, 647–664; V. Buß, M. Schreiber, M. P. Fülscher, *Angew. Chem.* **2001**, *113*, 3284–3286; *Angew. Chem. Int. Ed.* **2001**, *40*, 3189–3190.

[11] J. Fabian, H. Nakazumi, M. Matsuoka, *Chem. Rev.* **1992**, *92*, 1197–1226.

[12] N. Tyutyulkov, J. Fabian, A. Mehlhorn, F. Dietz, A. Tadjer, *Polymethine Dyes*, St. Kliment Ohridski University Press, Sofia, **1991**, pp. 128–137.

[13] F. Momicchioli, I. Baraldi, G. Berthier, *Chem. Phys.* **1988**, *123*, 103–112; I. Baraldi, A. Carnevali, F. Momicchioli, G. Ponterini, *Spectrochim. Acta Part A* **1993**, *49*, 471–495; M. L. Dekhtyar, W. Rettig, V. Rozenbaum, *J. Photochem. Photobiol. A* **1999**, *120*, 75–83; A. Sanchez-Galvez, P. Hunt, M. A. Robb, M. Olivucci, T. Vreven, H. B. Schlegel, *J. Am. Chem. Soc.* **2000**, *122*, 2911–2924; M. Dekhtyar, W. Rettig, M. Sczepan, *Phys. Chem. Chem. Phys.* **2000**, *2*, 1129–1136.

[14] S. A. Soper, Q. L. Mattingly, *J. Am. Chem. Soc.* **1994**, *116*, 3744–3752; J. E. H. Buston, J. R. Young, H. L. Anderson, *Chem. Commun.* **2000**, 905–906.

[15] R. C. Benson, H. A. Kues, *J. Chem. Eng. Data* **1977**, *22*, 379–383; M. Sczepan, W. Rettig, Y. L. Bricks, Y. L. Slominski, A. I. Tolmachev, *J. Photochem. Photobiol. A* **1999**, *124*, 75–84.

[16] K.-H. Drexhage, *J. Res. Natl. Bur. Stand. Sect. A* **1976**, *80*, 421–428; M. Vogel, W. Rettig, R. Sens, K. H. Drexhage, *Chem. Phys. Lett.* **1988**, *147*, 452–460; T. López Arbeloa, F. López Arbeloa, P. Hernández Bartolomé, I. López Arbeloa, *Chem. Phys.* **1992**, *160*, 123–130; S. A. Soper, H. L. Nutter, R. A. Keller, L. M. Davis, E. B. Shera, *Photochem. Photobiol.* **1993**, *57*, 972–977.

[17] D. F. O'Brien, T. M. Kelly, L. F. Costal, *Photogr. Sci. Eng.* **1974**, *18*, 76–84.

[18] The same generally applies for cyanines as well. However, within this class of dyes, uncharged merocyanines, for instance, often show a better solubility in a broader range of solvents.

[19] S. S. Malhotra, M. C. Whiting, *J. Chem. Soc.* **1960**, 3812–3822.

[20] H. Telle, W. Hüffer, D. Basting, *Opt. Commun.* **1981**, *38*, 402–406.

[21] T. G. Pavlopoulos, J. H. Boyer, M. Shah, K. Thangaraj, M.-L. Soong, *Appl. Opt.* **1990**, *29*, 3885–3886.

[22] a) E. Vos de Wal, J. Pardoen, J. A. van Koeveringe, J. Lugtenburg, *Recl. Trav. Chim. Pays-Bas* **1977**, *96*, 306–309; b) J. A. Pardoen, J. Lugtenburg, G. W. Canters, *J. Phys. Chem.* **1985**, *89*, 4272–4277; c) J. Karolin, L. B.-Å. Johansson, L. Strandberg, T. Ny, *J. Am. Chem. Soc.* **1994**, *116*, 7801–7806; d) R. W. Wagner, J. S. Lindsey, J. Seth, V. Palaniappan, D. F. Bocian, *J. Am. Chem. Soc.* **1996**, *118*, 3996–3997; e) M. Kollmannsberger, T. Gareis, S. Heinl, J. Breu, J. Daub, *Angew. Chem.* **1997**, *109*, 1391–1393; *Angew. Chem. Int. Ed. Engl.* **1997**, *36*, 1333–1335; f) F. Li, S. I. Yang, Y. Ciringh, J. Seth, I. C. H. Martin, D. L. Singh, D. Kim, R. R. Birge, D. F. Bocian, D. Holten, J. S. Lindsey, *J. Am. Chem. Soc.* **1998**, *120*, 10001–10017; g) T. López Arbeloa, F. López Arbeloa, I. López Arbeloa, I. García-Moreno, A. Costela, R. Sastre, F. Amat-Guerri, *Chem. Phys. Lett.* **1999**, *299*, 315–321; h) G. Beer, C. Niederalt, S. Grimme, J. Daub, *Angew. Chem.* **2000**, *112*, 3385–3388; *Angew. Chem. Int. Ed.* **2000**, *39*, 3252–3255; i) F. Bergström, I. Mikhalyov, P. Hägglöf, R. Wortmann, T. Ny, L. B.-Å. Johansson, *J. Am. Chem. Soc.* **2002**, *124*, 196–204; j) B. Turfan, E. U. Akkaya, *Org. Lett.* **2002**, *4*, 2857–2859; k) C. D. Entwistle, T. B. Marder, *Angew. Chem.* **2002**, *114*, 3051–3056; *Angew. Chem. Int. Ed.* **2002**, *41*, 2927–2931; l) A. Costela, I. García-Moreno, C. Gomez, R. Sastre, F. Amat-Guerri, M. Liras, F. López Arbeloa, J. Bañuelos Prieto, I. López Arbeloa, *J. Phys. Chem. A* **2002**, *106*, 7736–7742; m) R. Y. Lai, A. J. Bard, *J. Phys. Chem. B* **2003**, *107*, 5036–5042.

[23] In the context of the classification of polymethine systems put forward in reference [8b], BDPs are intrachain-coupled nonamethines. According to Dähne and Moldenhauer, such dyes possess a certain aromatic character and absorb at shorter wavelengths than their "ideal" analogues: the absorption maximum of the corresponding cycanine with $X=Y=N(CH_3)_2$ and $n=4$ is found at 625 nm.[12] For representative fluorescein dyes and their spectroscopic features, see G. R. Fleming, A. W. E. Knight, J. M. Morris, R. J. S. Morrison, G. W. Robinson, *J. Am. Chem. Soc.* **1977**, *99*, 4306–4311.

[24] M. P. Debreczeny, W. A. Svec, M. R. Wasielewski, *Science* **1996**, *274*, 584–587; T. Gareis, C. Huber, O. S. Wolfbeis, J. Daub, *Chem. Commun.* **1997**, 1717–1718.

[25] L. H. Thoresen, H. Kim, M. B. Welch, A. Burghart, K. Burgess, *Synlett* **1998**, 1276–1278; H. Kim, A. Burghart, M. B. Welch, J. Reibenspies, K. Burgess, *Chem. Commun.* **1999**, 1889–1890; A. Burghart, H. Kim, M. B. Welch, L. H. Thoresen, J. Reibenspies, K. Burgess, F. Bergström, L. B.-Å. Johansson, *J. Org. Chem.* **1999**, *64*, 7813–7819;

J. Chen, J. Reibenspies, A. Derecskei-Kovacs, K. Burgess, *Chem. Commun.* **1999**, 2501–2502; J. Chen, A. Burghart, A. Derecskei-Kovacs, K. Burgess, *J. Org. Chem.* **2000**, *65*, 2900–2906; A. Burghart, L. H. Thoresen, J. Chen, K. Burgess, F. Bergström, L. B.-Å. Johansson, *Chem. Commun.* **2000**, 2203–2204; J. Chen, A. Burghart, C.-W. Wan, L. Thai, C. Ortiz, J. Reibenspies, K. Burgess, *Tetrahedron Lett.* **2000**, *41*, 2303–2307.

[26] K. Yamada, T. Toyota, K. Takakura, M. Ishimaru, T. Sugawara, *New J. Chem.* **2001**, *25*, 667–669.

[27] a) K. Rurack, M. Kollmannsberger, J. Daub, *Angew. Chem.* **2001**, *113*, 396–399; *Angew. Chem. Int. Ed.* **2001**, *40*, 385–387; b) K. Rurack, M. Kollmannsberger, J. Daub, *New J. Chem.* **2001**, *25*, 289–292.

[28] A preliminary account of the synthetic procedure was published in M. Wada, S. Ito, H. Uno, T. Murashima, N. Ono, T. Urano, Y. Urano, *Tetrahedron Lett.* **2001**, *42*, 6711–6713.

[29] To better distinguish the chromophoric properties and owing to the fact that, from the spectroscopic point of view, the tetrahydrobisethano boron–diindomethenes are more closely related to the classical BDPs than to the fully aromatic BDIs, the tetrahydrobisethano derivatives are referred to and abbreviated as bicyclo-appended BDPs or bc-BDPs throughout the paper.

[30] a) M. Kollmannsberger, K. Rurack, U. Resch-Genger, J. Daub, *J. Phys. Chem. A* **1998**, *102*, 10211–10220; b) K. Rurack, M. Kollmannsberger, U. Resch-Genger, J. Daub, *J. Am. Chem. Soc.* **2000**, *122*, 968–969; c) M. Kollmannsberger, K. Rurack, U. Resch-Genger, W. Rettig, J. Daub, *Chem. Phys. Lett.* **2000**, *329*, 363–369; d) G. Beer, K. Rurack, J. Daub, *Chem. Commun.* **2001**, 1138–1139.

[31] S. Ito, T. Murashima, N. Ono, *J. Chem. Soc. Perkin Trans. 1* **1997**, 3161–3165.

[32] C. L. Picou, E. D. Stevens, M. Shah, J. H. Boyer, *Acta Crystallogr.* **1990**, *46*, 1148–1150.

[33] N. Kuhn, A. Kuhn, M. Speis, D. Blaser, R. Boese, *Chem. Ber.* **1990**, *123*, 1301–1303.

[34] B. Qian, S. W. Baek, M. R. Smith, III, *Polyhedron* **1999**, *18*, 2405–2414.

[35] V. Langer, H.-D. Becker, *Z. Kristallogr.* **1992**, *199*, 313–315.

[36] K. Goubitz, C. A. Reiss, D. Heijdenrijk, *Acta Crystallogr. Sect. C* **1989**, *45*, 1356–1358.

[37] Representative ground-state dipole moments as obtained from the quantum chemical calculations are for example, 3.8 D for **3a** and 2.1 D for **4a**.

[38] We have already studied some features of these dyes (J. L. Bricks, J. L. Slominskii, M. A. Kudinova, A. I. Tolmachev, K. Rurack, U. Resch-Genger, W. Rettig, *J. Photochem. Photobiol. A* **2000**, *132*, 193–208, compounds **8a–c** are equivalent to compounds **1a–c** in that paper), and they were reinvestigated here only as polymethine model systems. In the fits of the respective spectra of these cyanines **8a–c**, performed here for comparison, four species also had to be employed to describe the bands satisfactorily.

[39] The BDP (and the bc-BDP) chromophore can be considered as a cross-conjugated polymethine,[23] consisting of a trimethine and a nonamethine chain. On formal consideration, the BDI core constitutes a doubly cross-conjugated polymethine with an additional heptadecamethine chain.

[40] J. B. Birks, *Photophysics of Aromatic Molecules*, Wiley-Interscience, London, **1970**.

[41] $k_r = \Phi_f \tau_f^{-1}$ and $k_{nr} = (1-\Phi_f)\tau_f^{-1}$.

[42] G. Beer, M. Büschel, J. Daub, M. Kollmannsberger, B. König, G. Reck, H. Röhr, K. Rurack, Z. Shen, M. Subat, C. Trieflinger, unpublished results.

[43] The parameters derived from a global analysis of the fluorescence decay data and used in the present formalism are $\tau_1 = 3.39$ ns, $\tau_2 =$ 28 ps, $A_{11} = 2.68$, and $A_{12} = 23.4$ with $\tau_i =$ decay species and $A_{ij} =$ amplitudes.[30a] For further assumptions, the reader is also referred to reference [30a]. The photostationary state is reached after 188 ps. Similar to the findings for the *p*-dimethylamino derivative of **5a**,[30a] the process is not irreversible ($Y = 4.43 \times 10^9\ s^{-1}$ vs $Y^{irr} = 2.95 \times 10^8\ s^{-1}$). As pointed out by an attentive referee, there is a misprint in the denominator of Equation (16) of reference [30a] that should contain k_{CL} instead of k_{LC}.

[44] In accordance with the room-temperature behavior of **3b** in acetonitrile, no long wavelength CT emission band could be detected for **3b** in ethanol at 299 K or at any lower temperature.

[45] Phosphorescence could not be detected for any of the dyes at 77 K in the wavelength range up to 850 nm and at various delay times in the range of 0.05–100 ms with a Perkin–Elmer LS50B spectrometer with a low-temperature luminescence accessory, flash lamp excitation (fwhm < 10 μs), and gated PMT.

[46] This value lies in between the activation energies determined for the charge-transfer reactions connected with an intramolecular rotation coordinate of a less sterically hindered molecule such as *N,N*-dimethylaminobenzonitrile (4 kJ mol^{-1}; see K. A. Zachariasse, M. Grobys, T. von der Haar, A. Hebecker, Y. V. Il'ichev, Y.-B. Jiang, O. Morawski, W. Kühnle, *J. Photochem. Photobiol. A* **1996**, *102*, 59–70) and a more sterically hindered molecule such as 4-(2,6-dimethyl-4-*N,N*-dimethylaminophenyl)benzonitrile (14.3 kJ mol^{-1}; see M. Maus, W. Rettig, *J. Phys. Chem. A* **2002**, *106*, 2104–2111).

[47] $r = (F_{VV} - F_{VH})/(F_{VV} + 2F_{VH})$ with $r =$ anisotropy, $F =$ fluorescence intensity and subscripts V and H = vertically and horizontally aligned polarizers. Measurements above and below the glass point of ethanol at 170 and 140 K yielded very similar results in the case of **3b**.

[48] A. P. de Silva, H. Q. N. Gunaratne, T. Gunnlaugsson, A. J. M. Huxley, C. P. McCoy, J. T. Rademacher, T. E. Rice, *Chem. Rev.* **1997**, *97*, 1515–1566.

[49] The dimethylamino derivatives show a similar behavior, resulting in $\Phi_f = 0.67$ and $\tau_f = 5.76$ ns for **3b**-H$^+$ and $\Phi_f = 0.88$ and $\tau_f = 5.47$ ns for **4b**-H$^+$, respectively.

[50] Note that these experimental data are well reproduced by the theoretical data given in Section S1 of the Supporting Information.

[51] It is important to note that a theoretical analysis of the respective transitions in the ester-substituted bc-BDP chromophore revealed an even closer energetic spacing of the two lowest transitions as reported for the bc-BDP core above. Again, the $S_2 \leftarrow S_0$ transition involves the HOMO−1/−2 and LUMO with the former MOs being again largely localized on the bicyclo fragments (see Supporting Information). We thus tentatively assign the broad band on the high-energy side which overlaps considerably with the cyanine-type band to this transition and took this into account during spectral analysis.

[52] The biexponential decay of **4e** in MeOH is presumably caused by hydrogen bonding of solvent molecules to the benzocrown donor atoms.

[53] Note that the electrochemical data listed for **3f** in Table 6 do not show any peculiarities or hint at any such excited-state (quenching) reaction mechanism.

[54] a) B. Jahn, H. Dreeskamp, *Ber. Bunsen-Ges.* **1984**, *88*, 42–47; b) A kink angle of 13° in 9-*tert*-butylanthracene was determined by X-ray structure analysis.

[55] Although the model **3f** exhibits a much weaker fluorescence in methanol (0.008) than in apolar solvents, complexation of **3e** with Na$^+$ also leads to the expected increase in emission from a very low (0.001) to a low fluorescence yield (0.005).

[56] Unbound **4e** shows an additional narrow absorption band at 785 nm in aqueous solution, which is shifted to 825 nm in the presence of Na$^+$. The fluorescence of the latter species, occurring at $\lambda = 830$ nm, is narrow and rather resonant. As this behavior is not straightforward and thus cannot be readily exploited for analytical sensing applications, we will not discuss the aggregation phenomena of **4e** in detail here.

[57] K. Rurack, J. L. Bricks, B. Schulz, M. Maus, G. Reck, U. Resch-Genger, *J. Phys. Chem. A* **2000**, *104*, 6171–6188.

[58] F. Wada, H. Hirayama, H. Nakimi, K. Kikukawa, T. Matsuda, *Bull. Chem. Soc. Jpn.* **1980**, *53*, 1473–1474.

[59] J. P. Dix, F. Voegtle, *Chem. Ber.* **1980**, *113*, 457–459.

[60] G. M. Sheldrick, SHELX97, University Göttingen (Germany) **1997**.

[61] Molecular Structure Corporation, teXscan. single-crystal structure analysis software, **2000**.

[62] J. Olmsted, III, *J. Phys. Chem.* **1979**, *83*, 2581–2584.

[63] J. M. Drake, M. L. Lesiecki, D. M. Camaioni, *Chem. Phys. Lett.* **1985**, *113*, 530–534.

[64] D. F. Eaton, *Pure Appl. Chem.* **1988**, *60*, 1107–1114.

[65] D. N. Dempster, T. Morrow, R. Rankin, G. F. Thompson, *Chem. Phys. Lett.* **1973**, *18*, 488–492.

[66] J. R. Lakowicz, *Principles of Fluorescence Spectroscopy*, 2nd ed., Plenum, New York, **1999**, p. 52.
[67] U. Resch, K. Rurack, *Proc. SPIE-Int. Soc. Opt. Eng.* **1997**, *3105*, 96 – 103.
[68] J. Bourson, J. Pouget, B. Valeur, *J. Phys. Chem.* **1993**, *97*, 4552 – 4557; S. Fery-Forgues, M. T. Le Bris, J.-P. Guetté, B. Valeur, *J. Phys. Chem.* **1988**, *92*, 6233 – 6237.
[69] M. J. S. Dewar, E. G. Zoebisch, E. F. Healy, J. J. P. Stewart, *J. Am. Chem. Soc.* **1985**, *107*, 3902 – 3909.

Received: February 20, 2004
Revised: May 26, 2004
Published online: August 17, 2004

